Deep learning strategies for automatic fault diagnosis in photovoltaic systems by thermographic images

D. Manno, G. Cipriani, G. Ciulla, V. Di Dio, S. Guarino, V. Lo Brano

Department of Engineering

University of Palermo, Palermo, Italy

e-mail: donatella.manno@unipa.it, giovanni.cipriani@unipa.it, giuseppina.ciulla@unipa.it, vincenzo.didio@unipa.it, stefania.guarino@unipa.it, valerio.lobrano@unipa.it

Abstract

Losses of electricity production in photovoltaic systems are mainly caused by the presence of faults that affect the efficiency of the systems. The identification of any overheating in a photovoltaic module, through the thermographic non-destructive test, may be essential to maintain the correct functioning of the photovoltaic system quickly and cost-effectively, without interrupting its normal operation. This work proposes a system for the automatic classification of thermographic images using a convolutional neural network, developed via open-source libraries. To reduce image noise, various pre-processing strategies were evaluated, including normalization and homogenization of pixels, greyscaling, thresholding, discrete wavelet transform, and Sobel Feldman and box blur filtering. These techniques allow the classification of thermographic images of differen quality and acquired using different equipments, without specific protocols. Several tests with different parameters and overfitting reduction techniques were carried out to assess the performance of the neural networks: images acquired by unmanned aerial vehicles and ground-based operators were compared for the network performance and for the time required to execute the thermographic inspection. Our tool is based on a convolutional neural network that allows to immediately recognize a failure in a PV panel reaching a very high accuracy. Considering a dataset of 1000 images that refer to different acquisition protocols, it was reached an accuracy of 99% for a convolutional neural network with 30 minutes of computational time on Low Mid-Range CPU. While a dataset of 200 sectioned images, the same tool achieved 90% accuracy with a multi-layer perceptron architecture and 100% accuracy for a convolutional neural network. The proposed methodology offers an open alternative and a valid tool that improves the resolution of image classification for remote failure detection problems and that can be used in any scientific sector.

Keywords

Please cite this paper as:
D. Manno, G. Cipriani, G. Ciulla, V. Di Dio, S. Guarino, V. Lo Brano. (2021). Deep learning strategies for automatic fault diagnosis in photovoltaic systems by thermographic images. Energy Conversion and Management, 241, 114315.
https://doi.org/10.1016/j.enconman.2021.114315

Automatic Fault recognition, Convolutional Neural Network, Photovoltaics, TensorFlow, Infrared Thermography.

1. Introduction

Currently, fossil fuels are still a very important energy resource in the world, representing 79.7% [1] of electricity production. As it is known, fossil fuels require millions of years to form natural reserves such as coal, oil, and natural gas and the life-cycle of these resources is longer than the speed of their use in modern society, so they are destined to run out in the coming decades. Furthermore, the use of fossil fuels causes the emission of greenhouse gases that accelerate climate change via global warming, thereby threatening the environment and humankind [2]. In the last few years, to meet the energy needs of the world and simultaneously to protect the environment, the production of energy from renewable sources has been promoted thanks to the diffusion of innovative and efficient energy production systems reducing the emissions of sulfur (SO_2), carbon (CO_2) and dust, and decreasing the potential production of air pollution [3].

Renewable energy sources, therefore, cover an important position for the production of green electricity as an alternative to fossil fuels energy sources. For this reason, the exploration of renewable energy sources has been favored by many countries and supported both by national and international policies during the last decade [4]. Even today, although the proposed incentives from various nations are lower than in previous years [5], renewable technology is still being promoted at a political level through decarbonization and environmental sustainability objectives promoted by Agenda 2030 [6], including an increase of 32% in the production of green energy by 2030. On the other hand, the reduction of incentives leads to an increase in the payback time, which can increase even further in the case of loss of production due to undiagnosed defects. It is, therefore, necessary to intervene promptly in the event of a reduction in system performance [7] to reduce the power losses and make investments competitive on the market.

In 2019, renewable energy production is only 27.3% of the total, of which 2.8% is produced by photovoltaic (PV) systems, which represents the second-largest portion of renewable energy exceeded only by wind power systems [8]. At the end of 2019, a total of 627 GWp of installed PV systems had been reached and specifically, in Italy, 24 TWh of electricity was produced [9].

The performance of the solar cell depends on environmental conditions, such as air temperature, wind speed, and solar radiation, and parameters of cell construction material, such as the transmittance of

Please cite this paper as:
D. Manno, G. Cipriani, G. Ciulla, V. Di Dio, S. Guarino, V. Lo Brano. (2021). Deep learning strategies for automatic fault diagnosis in photovoltaic systems by thermographic images. Energy Conversion and Management, 241, 114315.
https://doi.org/10.1016/j.enconman.2021.114315

the glass roof, absorbance of silicious layer, etc. Particularly, the electrical performance of the solar cell depends mainly on the type of silicon used. The most common cells convert from 6 to 25% of the incident solar radiation into electrical energy, while the rest is converted into heat, resulting in a significant temperature increase of the module that reduces its efficiency [10].

In PV plants, electricity production losses are mainly caused by the presence of anomalies affecting the operation of the systems. An important cause of abnormal system operation is system failure [11], which not only causes a reduction in efficiency of PV systems but also represents an electrical risk for operators in the case of large PV systems or non-expert users in the case of small PV systems [12].

System monitoring is essential for determining performance degradation and identifying module health. The identification of degradation of the modules allows the maintenance of the correct functioning of the system, avoiding the production loss of electricity. PV systems consist of several modules and the balance of systems (all system components other than PV modules, such as wiring, switches, inverter, etc.), which could be potentially affected by faulty conditions [13]. Faults according to the affected parts of the PV system, can be divided into:

1) faults afflicting the module and the cells: breakage of the cell, hotspot, loss of adhesion and the consequent separation of the EVA encapsulant and the substrate film of the PV module, etc.;
2) and faults affecting the other components of the system: broken junction boxes, broken connections, etc.

Any anomaly in the operation of the solar cell causes an increase in its operating temperature and, this condition leads to a decrease in module efficiency and a reduction of solar radiation converted into electrical energy [14].

Anomalies can be varied [11] and can be related to events that limit the correct operation of the PV module occurring because of accidental or occasional causes (catastrophic failures), or degradations or degenerative phenomena that cause a progressive decrease in the functionality of the module increasing over the years.

Among the main causes of failure, the presence of hotspots is one of the most common [15]. A hotspot [16] is a degenerative phenomenon that occurs during the operation of the PV module (even in low

Please cite this paper as:
D. Manno, G. Cipriani, G. Ciulla, V. Di Dio, S. Guarino, V. Lo Brano. (2021). Deep learning strategies for automatic fault diagnosis in photovoltaic systems by thermographic images. Energy Conversion and Management, 241, 114315.
https://doi.org/10.1016/j.enconman.2021.114315

irradiation conditions) due to localized overheating of the modules. This phenomenon occurs when the operating current of the module is higher than the short-circuit current production of a cell [17], inducing the inverse polarization of the solar cell and, therefore, the loss of power as heat, causing a localized increase in the surface temperature, which can exceed 150°C [18]. High-temperature conditions, above the critical temperature, in the long term can cause a loss of the insulating properties of the module and eventually the delamination and breakage of the cells [18]. On the contrary, it was shown that even the temperature of the encapsulants of commercial modules can cause deterioration. The presence of an encapsulation crack can cause a hotspot due to the infiltration of moisture into the module [13]. Hotspot phenomena are attributed to several causes, such as partial or total shading of the cell, the shunt of the P-N junction of the cell due to impurities on the wafers or in the connection, the delamination of the cell, the presence of cracks, and cell breakage, etc [16].

To minimize the efficiency losses of the PV system, it is essential to observe and identify abnormal operating conditions. Faults can dramatically decrease system performance based on the type and the time required to diagnose them. For example, as indicated in [13], failures such as delamination (loss of adhesion between the glass, encapsulant, active layer, and back layer compromised) can cause an energy loss of 4%; cell breakage can cause an energy loss of between 4% and 10% proportional to the number of broken cells [19]; while entire modules short-circuited in a string can cause a major loss of energy production [20].

One of the common methods for diagnosing faults in PV systems is the Thermographic Non-Destructive Test (TNDT), which allows the examination of the operating conditions of the system using infrared thermography [21]. TNDT analysis enables the measurement of the cell temperature and the highlighting of areas of localized overheating in the module attributable to the hotspots thanks to the emission of infrared radiation based on the temperature of the material without directly accessing the module [22]. TNDT procedure elaborates, in fact, thermographic images that contain information about the surface temperature of the module in each pixel [21]. Temperatures between 1 and 10°C can be attributed to external factors, such as dust or soiling, while higher temperatures are associated with module failures [23]. In a thermographic image, a hotspot is identified by a part of the module surface (including one or more cells) characterized by a color corresponding to a higher temperature indicating localized overheating. Conversely, a thermographic image of an operating module shows the uniform color and, therefore, uniform temperature over the whole module surface. Unlike other methods [24], such as current-voltage characteristics detection [25] or other innovative

Please cite this paper as:
D. Manno, G. Cipriani, G. Ciulla, V. Di Dio, S. Guarino, V. Lo Brano. (2021). Deep learning strategies for automatic fault diagnosis in photovoltaic systems by thermographic images. Energy Conversion and Management, 241, 114315.
https://doi.org/10.1016/j.enconman.2021.114315

techniques like the use of xenon flash lighting systems [26], TNDT allows the analysis of the operating state of PV modules quickly without interrupting normal system operation and using low-cost equipment. While for the other types of tests, it is necessary to disconnect the module from the system, and it requires a long time to analyze large systems [21].

TNDTs can be performed manually by a ground-based qualified operator or by using an Unmanned Areal Vehicle (UAV) integrated with a miniature thermal image camera, which allows for the inspection of large sized systems in a few hours [27]. The analysis of the operating status of a PV system using TNDTs with UAVs remotely piloted and supported by the proposed methodology allows considerable timesaving compared to the execution of TNDTs manually performed by a ground-based operator. The use of UAVs saves 10 or 15 times the TNDT execution time compared to manual inspection [28]. The main parameters affecting the TNDT duration carried out with the support of UAVs are the size of the PV system; the flight altitude of UAV; and the flight characteristics, such as distance covered, speed, UAV turns. Large size PV systems contain a higher number of modules than small sized systems and, therefore, a longer time is required to carry out TNDT [29]. However, by varying the flight altitude of the UAV, it is possible to acquire thermographic images of several modules [30], reducing the number of images needed for the inspection of the entire PV system and consequently the time required to identify any anomalies in the normal operation [27]. Also, the extension of the PV system and the distance between the strings can influence the execution time of the TNDTs [30]. In [28] the execution of the TNDT following the technical standard IEC TS 62446-3: 2017 [31] allowed the inspection of the operating status of the PV modules with a time of 1.38 s/kWp for the “Stade de Suisse” PV plant in Bern, Switzerland and 1.73 s/kWp for the “Mont Soleil” PV plant in the Jura Mountains, Switzerland. The first site is made up of PV modules installed on the roof of the building with the same orientation; the second site, however, presents modules on the ground placed on 110 stands. In both cases, the different TNDT acquisition times can be explained by the different layout of the system, the route taken by the UAV, and the flight characteristics.

Afterwords, the inspection and recognition of the acquired thermographic images are performed by an experienced operator who repeatedly checks all the thermographic images [21]. As described in a case study of [30] for the manual inspection of thermographic images acquired by analyzing a PV system with a size of 36.7 MW, 9 days are required to recognize any abnormal operating status of the

Please cite this paper as:
D. Manno, G. Cipriani, G. Ciulla, V. Di Dio, S. Guarino, V. Lo Brano. (2021). Deep learning strategies for automatic fault diagnosis in photovoltaic systems by thermographic images. Energy Conversion and Management, 241, 114315.
https://doi.org/10.1016/j.enconman.2021.114315

PV modules. In order not to be affected by human error, this operation takes a long time and a consistently high level of attention.

To reduce human error and allow even an inexperienced operator, such as the owner of a domestic system, to identify the operating conditions of the PV system, it is possible to use an automatic classification system of thermographic images. In the literature, it is possible to find several methods for automatic input classification, such as Support Vector Machines (SVM) [32], Fuzzy logic [33], and Artificial Intelligence (AI) techniques like Deep Convolutional Neural Network (DCNN) [34] and Multy-Layer Perceptron (MLP) [35]. Since it is quite difficult to compare in an absolute way the performance of the classifiers [36], which are strongly dependent on the type, quality, and number of inputs [37]. Tab. 1 shows a comparison among the thermographic image classification technique available in the literature, considering the balance dataset tests. The application of AI could also be used in various sectors, specifically, in renewable sources, for the forecasting [38], management [39] and monitoring [40] of the parameters that affect the correct functioning of these systems, but also for the modelling and analysis of real system [41].

Table 1. Results found in relevant scientific literature concerning different thermographic image classification software.

	SVM [32]	Fuzzy [33]	DCNN [34]
Input number	1568	25	1622
Input resolution (dpi)	240 x 500	320 x 240	640 x 512
Network structure	5 predictors, 8 responses	3 triangular fuzzy membership with 27 Fuzzy IF-THEN rules	VGG-16 with stochastic gradient descent optimizer of 0.001 learning rate and a 0.9 momentum
Performance criteria	Cross Validation	-	Cross Entropy
Accuracy (%)	95.2	86	74

1.1 Contribution of the work

The paper proposes an automatic classification system made with open source software, to automatically classify the operating conditions of a PV module based on the training of thermal

Please cite this paper as:
D. Manno, G. Cipriani, G. Ciulla, V. Di Dio, S. Guarino, V. Lo Brano. (2021). Deep learning strategies for automatic fault diagnosis in photovoltaic systems by thermographic images. Energy Conversion and Management, 241, 114315.
https://doi.org/10.1016/j.enconman.2021.114315

anomalies shown in the thermographic images. In particular, a Convolutional Neural Network (CNN) was used to identify and classify thermographic images since the CNN is a highly reliable and replicable system even in cases where high-performance computation hardware is not available. The classification of PV modules is carried out using a general approach that classifies every PV thermographic image according to two categories: correctly functioning modules and defective modules, specifically hotspots. The CNN performance was assessed using several configurations and varying parameters, including augmentation and overfitting reduction techniques, and its validity was further confirmed by comparing the performance of CNN with that of an MLP. Furthermore, since the thermographic analysis carried out using UAV can be performed at different heights and positions in relation to the PV module, some positions of the UAVs may not make the PV operating status easily identifiable; therefore, the performance of CNN was compared using thermographic images obtained by a ground-based operator and UAV. The proposed tool allows, with a high level of accuracy, the immediate identification of a breakdown or malfunction avoiding important losses in electricity production, reducing the payback time of the solar plant.

The suggested detection system is attractive in various aspects:

- the proposed tool, using AI, is able to classify images that have been acquired at different PV sites without a standard protocol or specific camera equipment. Moreover, thanks to an innovative pre-processing phase of the images that are included in the input dataset of the neural network, consisting of the combination of different techniques to limit noise and information redundancy, and to highlight the features of the images, it is possible to obtain high levels of accuracy and the F-score regardless of the graphic quality of the collected images;
- the use of open-source deep learning frameworks, such as Tensorflow by Google, makes this application a low-cost tool that can be freely replicated by anyone;
- the proposed approach to solving the problem of image classification can be generalized and applied to studies and analyses conducted in different scientific areas, from engineering to medicine.

After a brief illustration of the typical malfunctioning conditions of PV systems, the paper proposes the use of TNDT to detect faults in a PV system and the application of artificial networks to classify thermographic images. To guarantee replicability, in this paper the entire numerical procedure is described, along with the description of the proposed CNN model and its construction. The results

Please cite this paper as:
D. Manno, G. Cipriani, G. Ciulla, V. Di Dio, S. Guarino, V. Lo Brano. (2021). Deep learning strategies for automatic fault diagnosis in photovoltaic systems by thermographic images. Energy Conversion and Management, 241, 114315.
https://doi.org/10.1016/j.enconman.2021.114315

confirm that the choice of CNNs represents an optimal and alternative solution for the classification of faults in PV technology.

2. Methods

To limit the energy loss and automatically examine the thermographic images, automatic classification software can be used. Classification is the ability to match at the category to a specific subject [42]. For humans, this ability is learned from childhood in which the mind is trained to identify a subject by its name, and using the same principle, an automatic classifier identifies a material with a unique label. Using AI, it is possible to create a general and flexible classification tool that can recognize information from images regardless of the quality, number of pixels, type, and acquisition device utilized to collect the images. A tool of this kind can be applied to the identification of hotspots of PV plants through the classification of modules thermographic images; it is possible to use AI systems. As is known, in fact, AI, by mimicking the behavior of the human brain [43], has a high capacity to identify input whatever its quality and characteristics, being able to recognize the specific patterns of the class despite there being [42]: distorted input, input of different sizes, different recognition patterns, deformed, superimposed or obscured by obstacle characteristics, or entrance rotated from any angle.

The classification of the thermographic images is achieved by providing images (acquired and pre-processed) as input to the AI, which is capable of identifying the category belonging to the subject [44], recognizing unique identification patterns [45]. Supervised learning [46] can be used to better perform the classification: during the training phase, a label representative of the category is assigned to the input image [47], while, during the AI test it receives the images of the corresponding subset without labels to check the quality of learning.

Among the different types of AI, this paper compares the performance of CNN and the more classic MLP [39]. CNN, realized by LeCun [48], is used in the literature with different applications [49] and exhibits more reliable behavior in image pattern recognition, while MLP has a simpler linear structure [35]. In the specific case of thermographic images, the classification is performed based on the operating status of the modules, in the categories “Operative” and “Hotspot”.

A hotspot in a thermographic image is highlighted by a module area, formed by one or more cells, which shows a localized overheating; conversely, an operating module exhibits the same uniform temperature on the module surface. A comparison between these two cases is shown in Fig. 1.

Please cite this paper as:
D. Manno, G. Cipriani, G. Ciulla, V. Di Dio, S. Guarino, V. Lo Brano. (2021). Deep learning strategies for automatic fault diagnosis in photovoltaic systems by thermographic images. Energy Conversion and Management, 241, 114315.
https://doi.org/10.1016/j.enconman.2021.114315

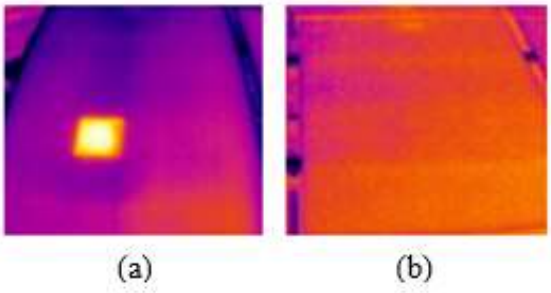

Fig. 1: PV with a hotspot (a) and operating PV (b).

The efficiency losses of the module and the consequent reduction in electric energy production caused by a hotspot are very variable and depend on the severity to which it occurs and its diffusion in the PV system. Fig. 2 shows hotspots of different severity and size: in (a) and (c) one cell is affected by hotspot, instead of in (b) two cells are involved.

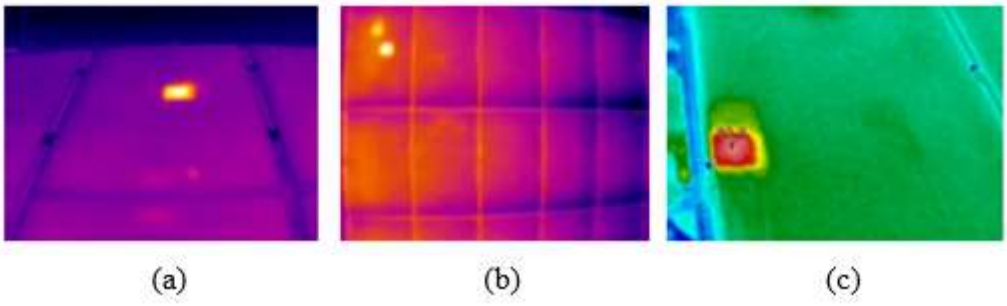

Fig. 2: Different hotspots highlighted by thermographic images.

The identification pattern is determined by the presence of edges and discontinuity in the brightness intensity values of the image pixels. To identify the specific patterns, CNN can be used to search image characteristics that recognize the input class. In Fig. 3, a representation of this process is shown.

Please cite this paper as:
D. Manno, G. Cipriani, G. Ciulla, V. Di Dio, S. Guarino, V. Lo Brano. (2021). Deep learning strategies for automatic fault diagnosis in photovoltaic systems by thermographic images. Energy Conversion and Management, 241, 114315.
https://doi.org/10.1016/j.enconman.2021.114315

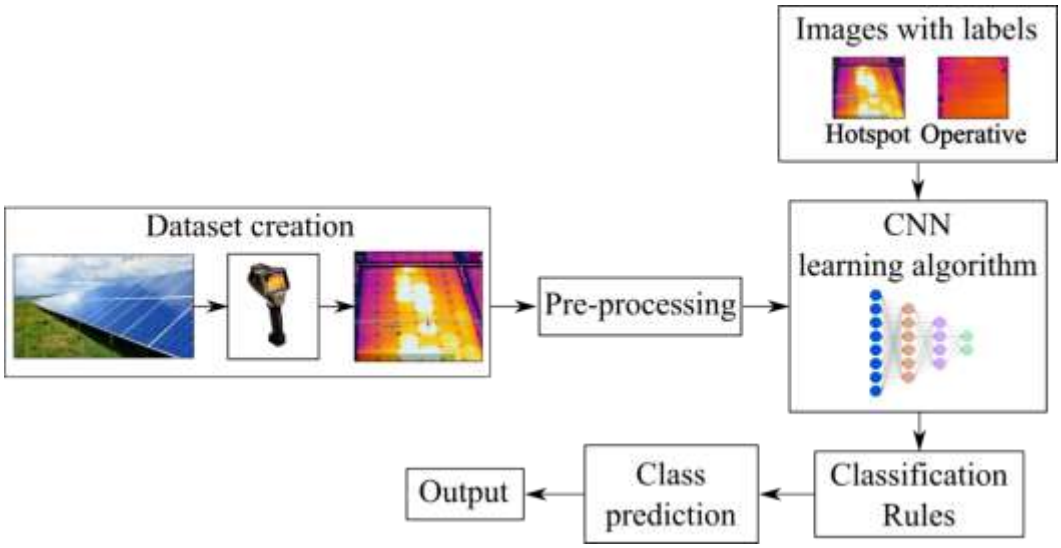

Fig. 3: Classification process.

The CNN is a feed-forward network [50] that presents a group of connected neurons inspired by the organization of the animal visual cortex [51]. As shown in Fig. 4, CNN is organized by alternating the following layers: a set of Convolutional and pooling layers, a flatten layer, and some completely connected layers. CNN consists of two stages: feature extraction and classification [47].

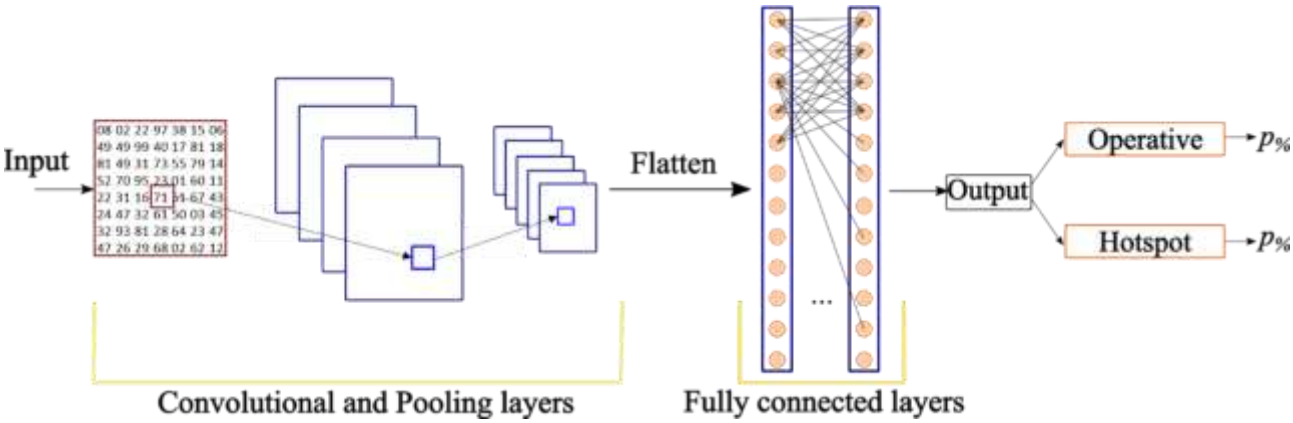

Fig. 4: Flow chart of CNN architecture.

The Convolutional and pooling layers identify the features of the input by subsampling the pixel performed by the product between the input matrix (image) and the convolution matrix (Kernel) for the entire input size. This function is shown between the $f(n)$ and $g(n)$ in Eq. 1. The Convolutional function is replicated for the entire section of the input matrix and returns a matrix, called the activation map, which contains the representative characteristics of the input [52].

Please cite this paper as:
D. Manno, G. Cipriani, G. Ciulla, V. Di Dio, S. Guarino, V. Lo Brano. (2021). Deep learning strategies for automatic fault diagnosis in photovoltaic systems by thermographic images. Energy Conversion and Management, 241, 114315.
https://doi.org/10.1016/j.enconman.2021.114315

$$(f \cdot g)[n] \overset{def}{=} \sum_{m=-\infty}^{\infty} f[m] \cdot g[n-m] = \sum_{m=-\infty}^{\infty} f[n-m] \cdot g[m] \quad (1)$$

The quality of the activation map depends on kernel size, kernel application step (stride), and padding, which is an artificial filling in the border of the input matrix to control the output volume. Zero-padding is generally used to ensure that the input and the output have the same size. Padding value, calculated in Eq. 2, depends on Kernel size (K) assuming Kernel strides (N) equal to 1.

$$P = \frac{K-1}{2} \quad (2)$$

The size of the activation map (W'), calculated by Eq. 3, depends on the input size (W), Kernel strides (N) , and padding value (P):

$$W' = \frac{W - K + 2 \cdot P}{N} + 1 \quad (3)$$

The Pooling layer is interposed between each Convolutional layer to sample the image by reducing the spatial size of the input and, therefore, the computing time. The pooling layer is combined with a mathematical function, such as Max-pooling, which approximates the features of the image by selecting the pixel with a maximum value [53].

The flatten function converts the output of the last Convolutional layer (matrix) to the input (vector) of the Fully connected layers. A Fully connected layer distinguishes the features represented by the activation maps and identifies the input class [54]. Each of these layers contains perceptrons that will be activated (learn) by the activation functions. Activation layers [55], as shown in Eq. 4, depend on the activation function type (s), a two-dimensional matrix containing the number of neurons in the previous and current layer (W), input vector (x), and bias vector (b).

$$s(W \cdot x + b) \quad (4)$$

The number of perceptrons of the Fully connected layers is related to the size of the input images since the inputs were convolved and pooled before the information arrived at the Fully connected layers. Thus, the number of perceptrons is calculated as 20% of the input size [56]. The activation

Please cite this paper as:
D. Manno, G. Cipriani, G. Ciulla, V. Di Dio, S. Guarino, V. Lo Brano. (2021). Deep learning strategies for automatic fault diagnosis in photovoltaic systems by thermographic images. Energy Conversion and Management, 241, 114315.
https://doi.org/10.1016/j.enconman.2021.114315

functions establish whether the perceptron is involved through the input information [57]. Particularly, the ReLU activation function is defined by Eq. 5:

$$s(x) = \max(0, x) \tag{5}$$

The output layer is used by the SoftMax activation function, which returns the probability that the input data belongs to each class [58]. This probability is examined by the cross-entropy loss module, which analyzes the image input and returns its category as the output. To make the neural network results replicable, the succession images used for the training phases not were randomized. For better performance, the CNN must be optimized by varying the configuration of various parameters that characterize it, such as optimizer, number of epochs, and batch size [59]. The optimizer improves the accuracy and speed of information convergence, the batch size is the number of samples propagated simultaneously through the CNN, while the number of epochs is the number of CNN learning cycles. Furthermore, CNN parameters must be chosen to limit the overfitting problem, which occurs when the learning algorithm adapts very well to the training data but does not correctly classify the new patterns coming from test data [60]. Several techniques can be used to reduce overfitting, including dataset augmentation techniques and the Dropout layer. The Dropout layer stochastically removes some inputs from the previous layer during the training step. Dropout is characterized by the likelihood of withholding neuron information; this avoids the adaptation of the neural network to the observed samples and simulates the decision-making process like that of the human brain [61].

In this research paper, CNN was used for the classification of thermographic images obtained by TNDT. CNN was developed in the Python programming language using Google's Tensorflow [62] and Keras [63] deep learning frameworks. Moreover, the MLP was built with the same logic as CNN in Peltarion Synapse, a commercial software [64]. In this tool, the classification system was developed through several steps, as shown in Fig. 5: images are collected in datasets and undergo pre-processing steps before being sent to CNN. Besides, CNN models and characteristics were chosen by conducting numerous tests and checking the results. The CNN model includes the identification of the most suitable architecture for the classification problem. The selection of the configuration includes the identification of the best performing parameters of CNN. The selection of the parameters and architectures that allow the attainment of high precision and stability of the neural network was carried out through various tests.

Please cite this paper as:
D. Manno, G. Cipriani, G. Ciulla, V. Di Dio, S. Guarino, V. Lo Brano. (2021). Deep learning strategies for automatic fault diagnosis in photovoltaic systems by thermographic images. Energy Conversion and Management, 241, 114315.
https://doi.org/10.1016/j.enconman.2021.114315

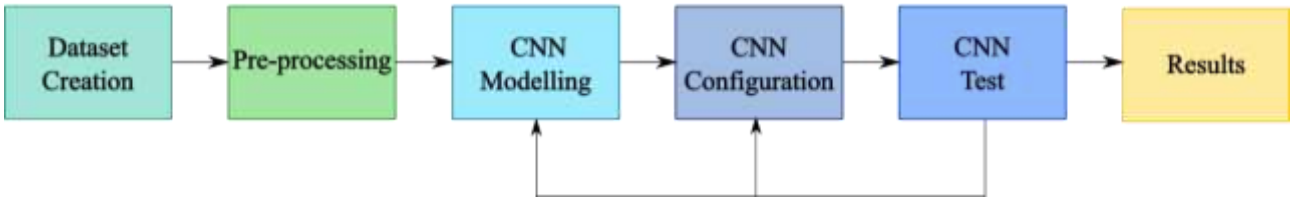

Fig. 5: Classification of system deployment steps.

2.1. Dataset creation

More than 4000 thermographic images were collected thanks to the collaboration of various companies. To generalize the application and enable it to classify any thermographic image without restrictions on quality, size, type, and acquisition technology, several thermographic images were used for the CNN training:

- thermographic images acquired manually by the operator or using UAVs;
- thermographic images acquired using different equipment of different characteristics (resolution, type of lens, distance from the module, orientation, etc.);
- thermographic images acquired from legacy technology modules (more than 10 years of operation) of different characteristics, located in different regions of Italy.

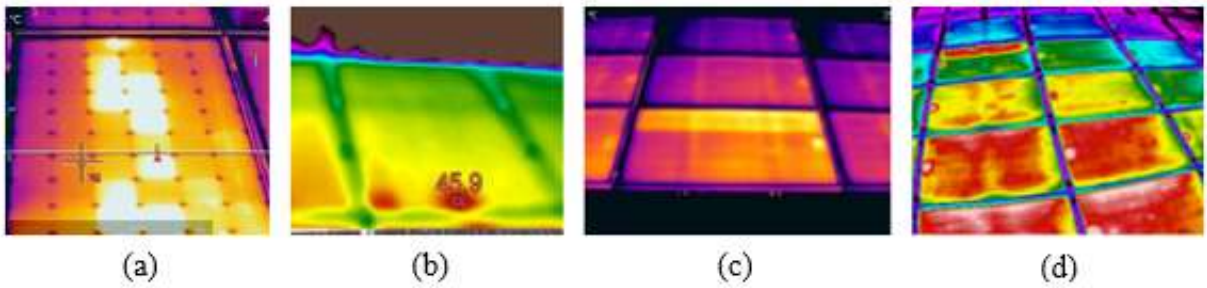

Fig. 6: Different thermographic images used.

Fig. 6 shows different thermographic images used for CNN training: in (a) the thermographic image has been acquired with a standard lens by an operator; in (b) the thermographic image has been acquired not perpendicular to the module; in (c) the thermographic image has been acquired with a standard lens and includes several PV modules; in (d) the thermographic image has been acquired with a wide-angle lens and includes several PV modules.

Balanced datasets, i.e. containing the same number of images for each category, with 500 and 1000 images were used to find the optimal configuration. Two datasets of 240 images were used to compare

Please cite this paper as:
D. Manno, G. Cipriani, G. Ciulla, V. Di Dio, S. Guarino, V. Lo Brano. (2021). Deep learning strategies for automatic fault diagnosis in photovoltaic systems by thermographic images. Energy Conversion and Management, 241, 114315.
https://doi.org/10.1016/j.enconman.2021.114315

the performance of CNN for images acquired by operators and UAVs. The datasets used for the test phase included images with different characteristics to avoid data mismatch. 20% of the images for the 1000 and 500 datasets and 33% of the images for the 240-image dataset were used. The thermographic images obtained with UAVs show the co-presence of several PV modules in the same frame, whose operating state is generally not identical, as shown in Fig. 7 in which a section of hotspot modules is indicated as "A", and an operating module as "B". To simplify the classification problem, sections of individual PV modules were made extracted from UAV images. In detail, a dataset of 200-sections was created, of which 15% were used for the test phase.

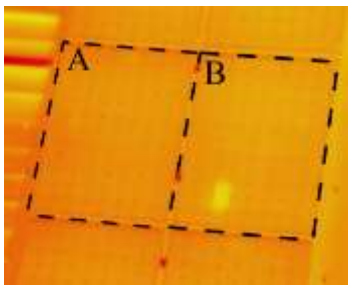

Fig. 7: Sectioning of thermographic images.

ImageDataGenerator from the Keras builder was used to provide the input dataset to CNN. This feature requires splitting the dataset into subfolders labeled by category to facilitate the supervised training phase [65]. It is a binary classification problem and the images are classified into two classes, "Operative" and "Hotspot". The breakdown of the dataset for the training and testing phases is shown in Tab. 2.

Table 2: Dataset split

	Acquisition image method	Number of images	Training data [%]	Test data [%]
Dataset 1	Operator	500	80	20
	UAV	1000		
Dataset 2	Operator	240	67	33
Dataset 3	UAV	240		
Dataset 4	Sections	200	85	15

Please cite this paper as:
D. Manno, G. Cipriani, G. Ciulla, V. Di Dio, S. Guarino, V. Lo Brano. (2021). Deep learning strategies for automatic fault diagnosis in photovoltaic systems by thermographic images. Energy Conversion and Management, 241, 114315.
https://doi.org/10.1016/j.enconman.2021.114315

2.2. Pre-processing phase

The performance of the classifier depends on the quality of the input images and their complexity. A high-performance classifier should be able to achieve excellent results even when the input images show the same subject but vary in: point of view, lighting level, framing, subject, or background distortion [66]. Performance improvement is ensured by image pre-processing to reduce unhelpful information, noise, and data redundancy. A thermographic image of a PV module shows information related to the surface distribution of the heat flux, and operating anomalies can be attributed to a hotspot. An incorrect TNDT procedure could lead to the detection of a reflex than an unskilled user might wrongly recognize as a hotspot. The pre-processing techniques allow the correct classification of these errors, obtaining a homogeneous set of images. The pre-processing phases, as shown in Fig. 8, include the phase of removing any parts of the images not inherent to the subject, the standardization of the dimensions of the images respecting their proportions, and the normalization of the pixel intensity values to the maximum. This process increases the speed of neural network convergence during the training phases.

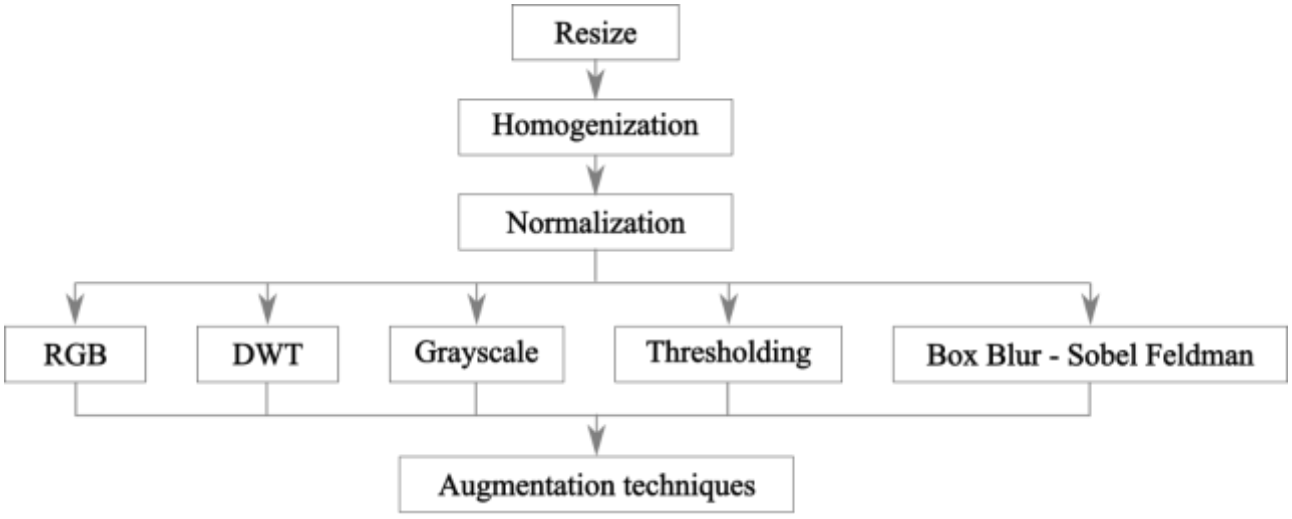

Fig. 8: Flow chart of pre-processing phases.

After the Normalisation phase, it is possible to choose among RGB color, Discrete Wavelet Transform (DWT), Grayscale, Thresholding, and a combination of Box Blur and Sobel Feldman filters. An application of these steps in the hotspot image is shown in Fig. 9.

The RGB pixel of the images is composed of a combination of Red, Green and Blue [67]. The color of thermographic images is a false color in the violet scale obtained from the default color scale settings, which depend on the thermal imaging camera brand and model used for TNDT. Since the

Please cite this paper as:
D. Manno, G. Cipriani, G. Ciulla, V. Di Dio, S. Guarino, V. Lo Brano. (2021). Deep learning strategies for automatic fault diagnosis in photovoltaic systems by thermographic images. Energy Conversion and Management, 241, 114315.
https://doi.org/10.1016/j.enconman.2021.114315

classification of the images is based on the recognition of the geometric shape of the hotspot, the color is considered unnecessary information [68]. The Grayscale processing allows image color to be converted to scale from white to black including shades of grey [67]. With DWT, the image characteristics are acquired by using low-pass and high-pass filters applied in different directions to obtain: approximation, horizontal, vertical, and diagonal detail images [69]. High-pass filters discriminate superficial image discontinuities (edges), meanwhile, low-pass filters remove pixel regions that have a lower extension compared to the filter mask [70]. The use of Thresholding tries to improve image discontinuities, a binarization of the black and white pixel intensity values is performed [66], and to improve the quality of the information, dilate and erode filters can be applied [69]. While the dilate filter determines the local maximum of pixel light intensity values to increase the brightest areas of the image (white), the erode filter determines the local minimum of pixel light intensity values to increase the less bright areas of the image (black).

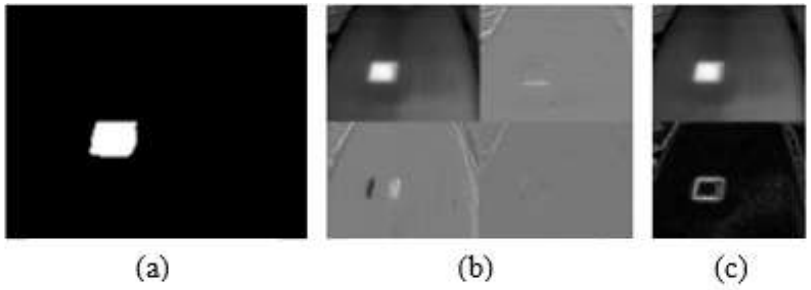

Fig. 9: Thresholding (a), DWT (b), Box blur and Sobel Feldman filters (c).

The Sobel Feldman filter [71] is a high-pass filter that discriminates the edges of the image by evaluating the gradient of a function representing the brightness values of pixels. The Sobel Feldman filter is applied with a kernel convolution called the Sobel Feldman mask. The kernel is applied in both vertical and horizontal directions and has a size of 3 x 3 to maintain symmetry at the central point of the image. Finally, the Box Blur filter [72] is a low-pass filter, i.e. a spatial domain linear filter, which can blur the image to reduce its discontinuities by converting the input image pixels into its average near-pixel value. The Box Blur filter is a linear media filter used to reduce noise in the image by removing irrelevant details, i.e. regions of pixels that have small extensions compared to the mask size of the filter. This filter elicit the core object as edges. The Box blur and Sobel Feldman filers are combined into one image; the application of these filters can be used in opposition to DWT.

Please cite this paper as:
D. Manno, G. Cipriani, G. Ciulla, V. Di Dio, S. Guarino, V. Lo Brano. (2021). Deep learning strategies for automatic fault diagnosis in photovoltaic systems by thermographic images. Energy Conversion and Management, 241, 114315.
https://doi.org/10.1016/j.enconman.2021.114315

Another type of pre-processing is the augmentation technique [73], which allows the number of training samples to be artificially increased so that the algorithms can discriminate input noise and detect data features more efficiently. The augmentation techniques increase the number of images present in the input dataset by automatically generating artificial data, using roto-translation and zoom applications in the original image randomly [74]. An example of these techniques, such as translation, flipping (c), rotation (d), and zooming (b), applied to the original image (a) is shown in Fig. 10.

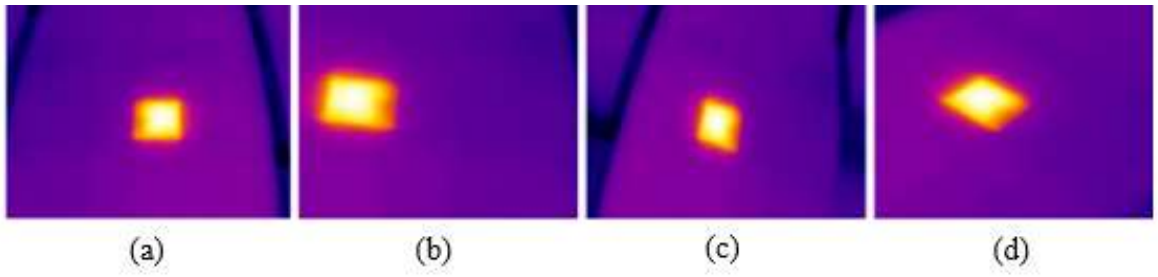

Fig. 10: Examples of augmentation techniques; original image (a), zooming (b), flipping (c), rotation (d).

2.3. Convolutional neural network model and configuration

To evaluate the best performing CNN for the classification of thermographic images, the neural network was carried out with different models and a minimum number (equal to 3) of Convolutional layers employed by *Conv2D* object of Keras library. According to the image features, Max-pooling was used to univocally distinguish the pixel intensity values and select the highest value and was implemented using the *MaxPooling* object provided via the Keras library. From the same library, the *Dense* object was used to realize Fully connected layers that return an output vector size equal to 2; each element of the last vector represents the probability that input belongs to one class. The Dropout layer was deployed via the *Dropout* object of Keras, using a holding probability of 10%. Lastly, the following models of CNN were implemented:

- Model "0" is composed of three Convolutional layers alternating with layers of pooling, followed by a Flatten layer and two Fully connected layers;
- Model "1" is composed of four Convolutional layers alternating with layers of pooling, followed by a Flatten layer and two Fully connected layers;
- Model "2" presents three Convolutional layers alternating with layers of pooling, followed by a Flatten layer, a Fully connected layer, a Dropout layer, and two Fully connected layers, as shown in Fig. 11.

Please cite this paper as:
D. Manno, G. Cipriani, G. Ciulla, V. Di Dio, S. Guarino, V. Lo Brano. (2021). Deep learning strategies for automatic fault diagnosis in photovoltaic systems by thermographic images. Energy Conversion and Management, 241, 114315.
https://doi.org/10.1016/j.enconman.2021.114315

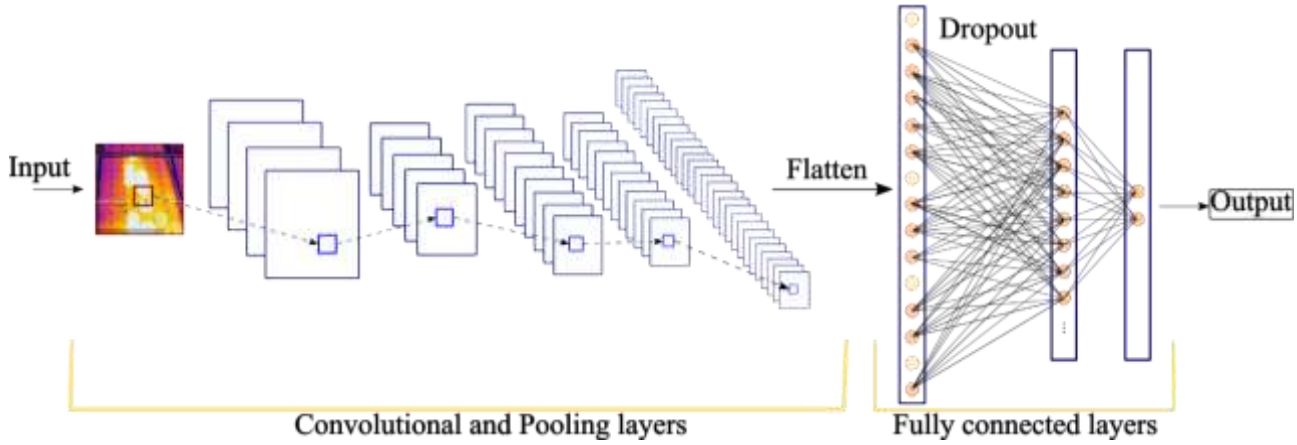

Fig. 11: Flow chart of model "2".

- Model "3" and "4" consist of the same structure as model "0", but in this case the Fully connected layer Sigmoid and Hyperbolic tangent activation functions were used.

For Convolutional layers and the Fully connected layers of models "0", "1" and "2" the ReLU activation function was used, while the SoftMax activation function was used for all the models in the output layer. Among the various CNN configurations, the one with the best compromise between stability and high performance, reducing the overfitting problem, was chosen.

The various CNN configurations differ in image sizing, number of perceptrons, number of epochs, hyperparameters related to Convolutional layers, activation functions, optimizers, learning rate, batch size, loss function, and metrics. The image sizes of 375 px, 3 kpx, and 12 kpx were chosen. The low values were set to keep low the training speed of the CNN by limiting the amount of information sent to the layers; the high value, instead, was selected to estimate the performance of CNN at increasing numbers of samples. The number of epochs of 30, 60, and 120 were chosen, as a result of different tests to limit the overfitting and underfitting (missed stability) of the CNN. The batch size was chosen at value of 5 or 10 integer multiples of the number of inputs, according to the performance of the used Low Mid -Range CPU. The optimizer was set according to the quality, the speed of convergence, and the computational time of the test execution. In particular, Adam and Stochastic Gradient Descent (SGD) optimizers were compared, both with a learning rate of 0.01. Hyperparameters related to the Convolutional layer concern kernel size, number of filters, stride, and padding. To identify the features of the image, 3 x 3 and 5 x 5 kernels with a single stride were used. The kernel size was set to evaluate the image features limiting data loss. Indeed, the images belonging to the "Hotspot"

Please cite this paper as:
D. Manno, G. Cipriani, G. Ciulla, V. Di Dio, S. Guarino, V. Lo Brano. (2021). Deep learning strategies for automatic fault diagnosis in photovoltaic systems by thermographic images. Energy Conversion and Management, 241, 114315.
https://doi.org/10.1016/j.enconman.2021.114315

category contain the co-presence of pixel regions identifiable as “Operative” which can determine a misclassification due to hotspot data loss. The number of filters was chosen according to the depth (number of layers) of the CNN. Since the Convolutional layers closer to the input learn fewer filters, while the following ones learn more, an increasing number of filters were chosen for each Convolutional layer. In detail, 16 and 32 filters were used for the first layer and doubled for the following layers. A zero-padding layer was added to limit the data loss of the image boundary maintaining the output size of the convolutional layer equal to the input. The loss function employed is sparse categorical cross-entropy that is most commonly used for classification problems.

2.4. Error Analysis

In machine learning, several metrics can be used to measure the performance of algorithms and evaluate classification errors for each class. To evaluate the predictive performance of the proposed CNN, the confusion matrix, accuracy (A), recall (R), f-score (FS) [75], and Receiver Operating Characteristic (ROC) space were calculated. The confusion matrix identifies samples as true positives (TP) and true negatives (TN), in which real and predicted class match; false positives (FP) and false negatives (FN), in which real and predicted class does not match. As shown in Eq. 6, CNN accuracy was obtained from a ratio of the sum of true positives and true negatives to the number of total predictions. The error was evaluated as a complement of the A value to one.

$$A = \frac{TP + TN}{TP + FP + FN + TN} \tag{6}$$

The recall is the capacity of the classifier to identify correctly all inputs belonging to a category. For binary classification, the parameter for classes 0 and 1 is determined by Eq. 7.

$$R(0) = \frac{TP(0)}{TN(0) + FN(0)}; \quad R(1) = \frac{TN(1)}{TP(1) + FP(1)} \tag{7}$$

The F-score parameter (FS), shown in Eq. 8, is a measure of model accuracy and is calculated with the average of accuracy and recall for each class. The arithmetic means of the FS values for both categories (FS_{AVG}) were evaluated.

$$FS = \frac{2 \cdot R \cdot A}{R + A} \tag{8}$$

During the tests, the standard deviation of the f-score was calculated for each parameter of CNN.

Please cite this paper as:
D. Manno, G. Cipriani, G. Ciulla, V. Di Dio, S. Guarino, V. Lo Brano. (2021). Deep learning strategies for automatic fault diagnosis in photovoltaic systems by thermographic images. Energy Conversion and Management, 241, 114315.
https://doi.org/10.1016/j.enconman.2021.114315

The CNN error analysis allows a benchmark to be determined for the performance of the classification of each class the best performing configuration using the ROC space. The graph of the ROC space presents the R-value on the ordinate and False Positive Rate (FPR) on the abscissa [76]. The FRP indicates the ability of the classifier to misidentify inputs belonging to a category and is determined, for classes 0 and 1, by Eq. 9.

$$\mathrm{FPR}(0) = \frac{\mathrm{FP}(0)}{\mathrm{FP}(0)+\mathrm{TN}(0)};\ \mathrm{FPR}(1) = \frac{\mathrm{FP}(1)}{\mathrm{FP}(1)+\mathrm{TN}(1)} \tag{9}$$

The prediction results of the confusion matrix can be represented by a point in ROC space. For two-class classification, the point (0, 1) is the perfect classification, called the high-sensitivity operating point, as there is no classification error. The diagonal line through the points (0, 0) and (1, 1) indicates the Non-Discrimination Line (NDL), which is representative of random results: the points above the diagonal are better than random results, while those below are worse.

3. Results

A total of 1316 tests were performed using different parameters, datasets and CNN configurations; another 6 tests were performed using MLP. Datasets of 500 and 1000 images were used to find the best CNN configuration by varying numerous parameters in ascending order. Tests on a dataset of 240 images were performed to compare CNN performance using images acquired by UAV and ground-based operators; the same tests were replicated using augmentation techniques. Finally, tests were carried out using the 200-images section dataset comparing CNN and MLP performance. For each test, during the CNN training and test phases, the computing time was evaluated in seconds.

3.1. Results using 500 images dataset

In total, 360 different CNN configurations of the 500 images dataset were tested by varying the types of pre-processing (Color, Grayscale, Thresholding, Wavelet, Sobel Feldman, Box Blur and Sobel Feldman); the epoch number (30, 60, 120); the optimizer (SGD, Adam) and model (0, 1, 2, 3, 4) type; the batch (5, 10) and image size (3024, 12096); and the kernel (3, 5) and filter size ({16, 32, 64, 128}, {32, 64, 128, 256}).

Table 3 shows the parameters used for the implementation of CNN with a lower standard deviation (relative to the f-score parameter averaged in the two classes). The Thresholding had a high FS_{AVG} value with a standard deviation of 0.01, representative of a consistently high prediction ability of

Please cite this paper as:
D. Manno, G. Cipriani, G. Ciulla, V. Di Dio, S. Guarino, V. Lo Brano. (2021). Deep learning strategies for automatic fault diagnosis in photovoltaic systems by thermographic images. Energy Conversion and Management, 241, 114315.
https://doi.org/10.1016/j.enconman.2021.114315

CNN across all 60 tests where pre-processing was used. Considering a compromise between stability and processing time, 60 epochs were set instead of 120. Moreover, 120 epochs often involved overfitting.

The Adam optimizer had a lower FS_{AVG} of 16.5% and a higher standard deviation than SGD, but high accuracy values can also be obtained thanks to the positive combination of parameter uncertainty using Adam. Model "1" had the highest FS_{AVG} value compared to model "0" of 0.19% and the same standard deviation. Models "2", "3", and "4" achieved lower FS_{AVG} values of 14.06%, 4.6%, and 5.93% respectively than model "1", resulting in fewer tests with high accuracy values. The 12096 image size had a lower FS_{AVG} value of 15.38% than the images of 3024.

Table 3: 500-image dataset best parameters.

Configuration	Parameters	FS_{AVG}	Standard Deviation
Pre-processing	Thresholding	0.94	0.01
Epochs	120	0.72	0.76
	60	0.70	0.27
Optimizer	SGD	0.77	0.12
Model	1	0.74	0.03
	0	0.73	0.03
Image size	3024	0.76	0.02

The maximum accuracy values reached was 97% as reported in Tab. 4. The parameters used for this test allowed a perfect classification of the images in the "Hotspot" class and an accuracy of 96% for the "Operative" class. The best high-performance stability parameters were obtained, achieving an accuracy value of 96% and a classification error of 4% for each class. It is important to underline that, the tests of shorter duration, of about a few minutes, were obtained using a number of epochs equal to 60, SGD optimizer, and 3024 pixels while the tests with 12096 pixels required longer computational time, but provided higher precision values.

Table 4: An extract of results with best performances.

Please cite this paper as:
D. Manno, G. Cipriani, G. Ciulla, V. Di Dio, S. Guarino, V. Lo Brano. (2021). Deep learning strategies for automatic fault diagnosis in photovoltaic systems by thermographic images. Energy Conversion and Management, 241, 114315.
https://doi.org/10.1016/j.enconman.2021.114315

Pre-processing	Epochs	Optimizer	Model	Image size	Duration (s)	Confusion Matrix				Accuracy
						TP	FP	FN	TN	
Thresholding	30	Adam	1	12096	635	47	3	0	50	0.97
Thresholding	60	SGD	0	3024	263	48	2	2	48	0.96
Thresholding	60	SGD	2	3024	533	48	2	2	48	0.96
						Operative		Hotspot		

In the ROC space shown in Fig. 12, CNN achieved high classification performance for 87% of the total tests, reaching the high-sensitivity operating point. 12% of the total tests, especially with the Adam optimizer and 12096 images size (in color or pre-processed in grayscaling and DWT), are displayed on the graph at points (1,1) and (0.5, 0) as they result in random performance or worse, due to Adam optimizer induced errors combined with noisy images. On the other hand, 1% of the tests are represented by the other points below the NDL, which can be explained by the stochasticity present in the SGD optimizer.

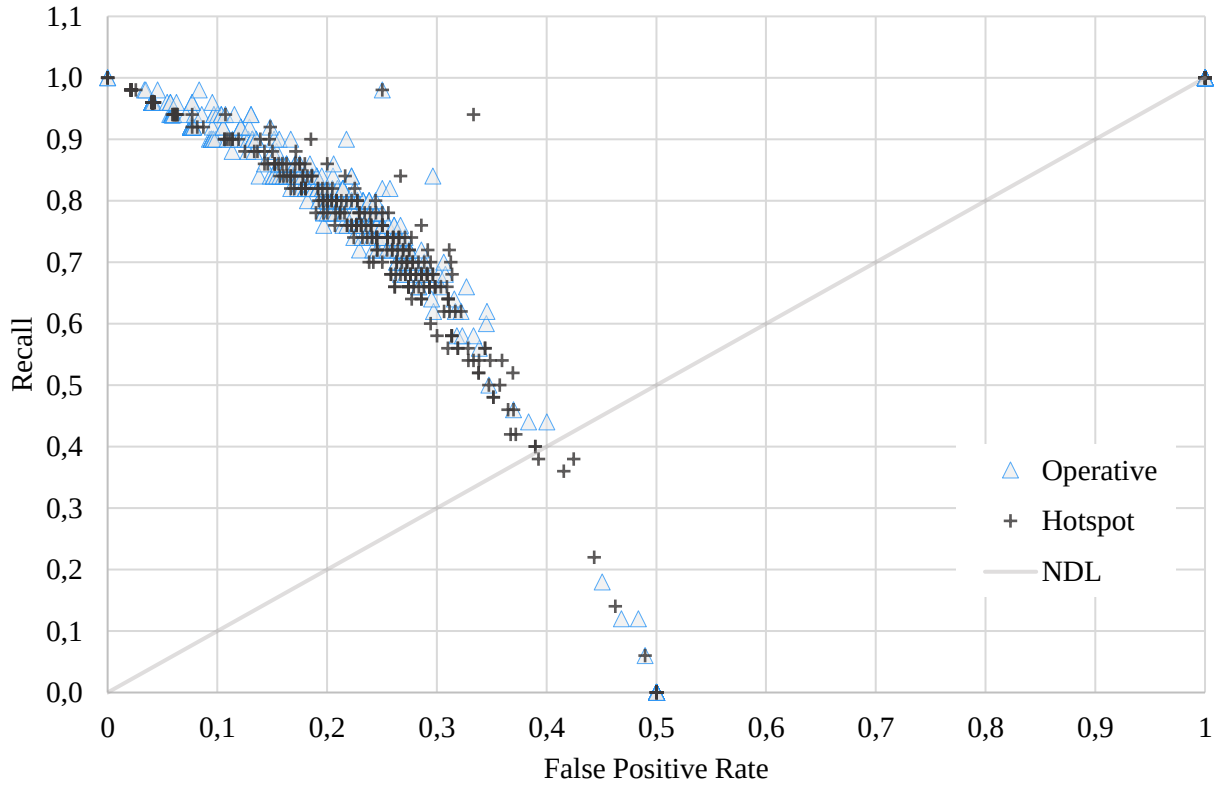

Please cite this paper as:
D. Manno, G. Cipriani, G. Ciulla, V. Di Dio, S. Guarino, V. Lo Brano. (2021). Deep learning strategies for automatic fault diagnosis in photovoltaic systems by thermographic images. Energy Conversion and Management, 241, 114315.
https://doi.org/10.1016/j.enconman.2021.114315

Fig. 12: ROC space for 500-image dataset.

3.2. Results using 1000-image dataset

The parameters and number of images used to perform these tests were set from the results shown in section 4.1. Datasets of 1000 pre-processed images in Thresholding were tested with 320 different configurations by varying: the number of epochs (30, 60), the type of optimizer (SGD, Adam), the model type (0, 1, 2, 3, 4), batch size (5, 10), image size (3024, 12096), kernel size (3, 5) and filter size ({16, 32, 64, 128}, {32, 64, 128, 256}). The batch size, kernel size, and filter size were increased compared to previous tests, in order to assess the classification ability of the CNN by increasing the image size and the input parameters. Overall, 300 configurations are characterized by accuracy values greater than 90%, and 244 of these show values greater than or equal to 95%, while 4 configurations have an accuracy close to 99%. The high accuracy values of the CNN configuration are collected in Tab. 5. The configuration used in the first row allows the correctly classification of all "Hotspot" images, achieving an accuracy of 100% for the class and 97% for the "Operative" class. The batch size, kernel size, and the number of filters affect the computing time of the test, increasing it by up to 10 minutes; the lower computational time is related to the configurations with 30 epochs, 10 batch sizes, 3 kernel sizes, and 16 filters.

Table 5: Extract of high accuracy tests.

									Confusion Matrix				
pp	e	opt	m	b	img	k	f	Duration (s)	TP	FP	FN	TN	Accuracy
TH	30	Adam	1	5	12096	3	32	2066	97	3	0	100	0.99
TH	60	Adam	1	10	12096	3	32	2757	99	1	2	98	0.99
TH	60	Adam	1	10	12096	5	32	3791	98	2	1	99	0.99
TH	60	Adam	4	5	12096	5	32	7100	100	0	3	97	0.99
TH	30	Adam	3	5	12096	5	16	1832	100	0	4	96	0.98
									Operative		Hotspot		

Legend: *pp = pre-processing, e = number of epochs, opt = optimizer, m = model, b = batch size, img = image size, k = kernel size, f = filter size, TH = thresholding*

Please cite this paper as:
D. Manno, G. Cipriani, G. Ciulla, V. Di Dio, S. Guarino, V. Lo Brano. (2021). Deep learning strategies for automatic fault diagnosis in photovoltaic systems by thermographic images. Energy Conversion and Management, 241, 114315.
https://doi.org/10.1016/j.enconman.2021.114315

The high performance achieved by CNN is mainly linked to the composition of the dataset and the parameters used for the tests. In the ROC space in Fig. 13 the CNN achieves very high performances, with accuracy greater than 90% for 84% for the tests performed, in 1% of cases reaching the high-sensitivity operating point for both classes. Instead, as for the dataset of 500 images, 16% of the total number of tests carried out using the Adam optimizer and images of size 12096 produced random or worse performance results identified at points (1,1), (0.5,0), (1, 0.5).

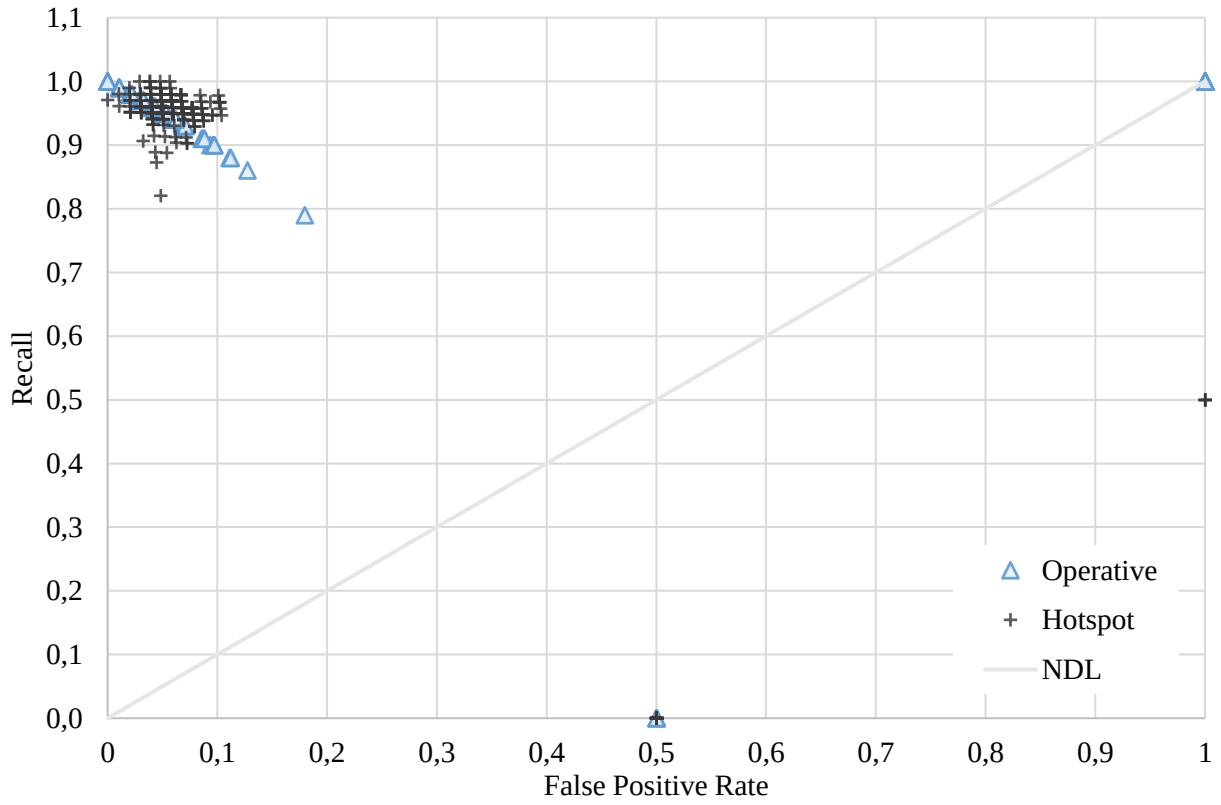

Fig. 13: ROC space for 1000-image dataset.

The parameters that allowed the attainment of a lower standard deviation (relative to the f-score parameter averaged on the two classes) are shown in Tab. 6.

Table 6: 1000-image dataset best parameters.

Configuration	Parameters	FS_{AVG}	Standard Deviation
Epochs	30	0.90	1.65
	60	0.88	3.06

Please cite this paper as:
D. Manno, G. Cipriani, G. Ciulla, V. Di Dio, S. Guarino, V. Lo Brano. (2021). Deep learning strategies for automatic fault diagnosis in photovoltaic systems by thermographic images. Energy Conversion and Management, 241, 114315.
https://doi.org/10.1016/j.enconman.2021.114315

Optimizer	SGD	0.94	0.16
Model	4	0.93	0.95
Image size	3024	0.91	0.98
	12096	0.87	3.43
Batch size	5	0.89	1.90
Kernel size	3	0.90	0.46
Filter size	{16, 32, 64, 128}	0.91	1.37

The number of epochs that resulted in a constant CNN response is 30 which presents an FS_{AVG} value of 1.42%. This value was greater than at 60 epochs and had a lower standard deviation. As in the test performed using the dataset of 500 images, the Adam optimizer allowed greater precision from the positive combination of the uncertainty of the parameters, with an FS_{AVG} value lower than SGD of 10.19%, and a standard deviation of 3.38. The FS_{AVG} value for batch sizes 5 and 10 differs by 0.18%, but the standard deviation of the second is greater. Image size, kernel size, and filter size had higher values of FS_{AVG} in the configurations 3024, 3, and {16, 32, 64, 128}, but the standard deviation of the 12096, 5 and {32, 64, 128, 256} values was high in the range of 3.18 and 3.43. Fig. 14 shows the accuracy and loss trends as a function of the number of epochs for the test performed using: thresholding pre-processing, 30 epochs, Adam optimizer, model "1", 3 batch size, 5 kernel size, 32 filters, and 12096-image size. In the training phase, image classification achieved the best classification performance after 10 epochs, as indicated by the constant traits in the accuracy and loss trends. The overfitting is underlined by the divergence of the loss function of the test in the training phases, due to the large size of the images and the use of the Adam optimizer. For the test phase, the accuracy trend reached the first stable range between 14 and 25 epochs with an accuracy value of 0.98, the second stable range occurs after 26 epochs. The loss trend, on the other hand, reached an almost constant trend after epoch 10.

Please cite this paper as:
D. Manno, G. Cipriani, G. Ciulla, V. Di Dio, S. Guarino, V. Lo Brano. (2021). Deep learning strategies for automatic fault diagnosis in photovoltaic systems by thermographic images. Energy Conversion and Management, 241, 114315.
https://doi.org/10.1016/j.enconman.2021.114315

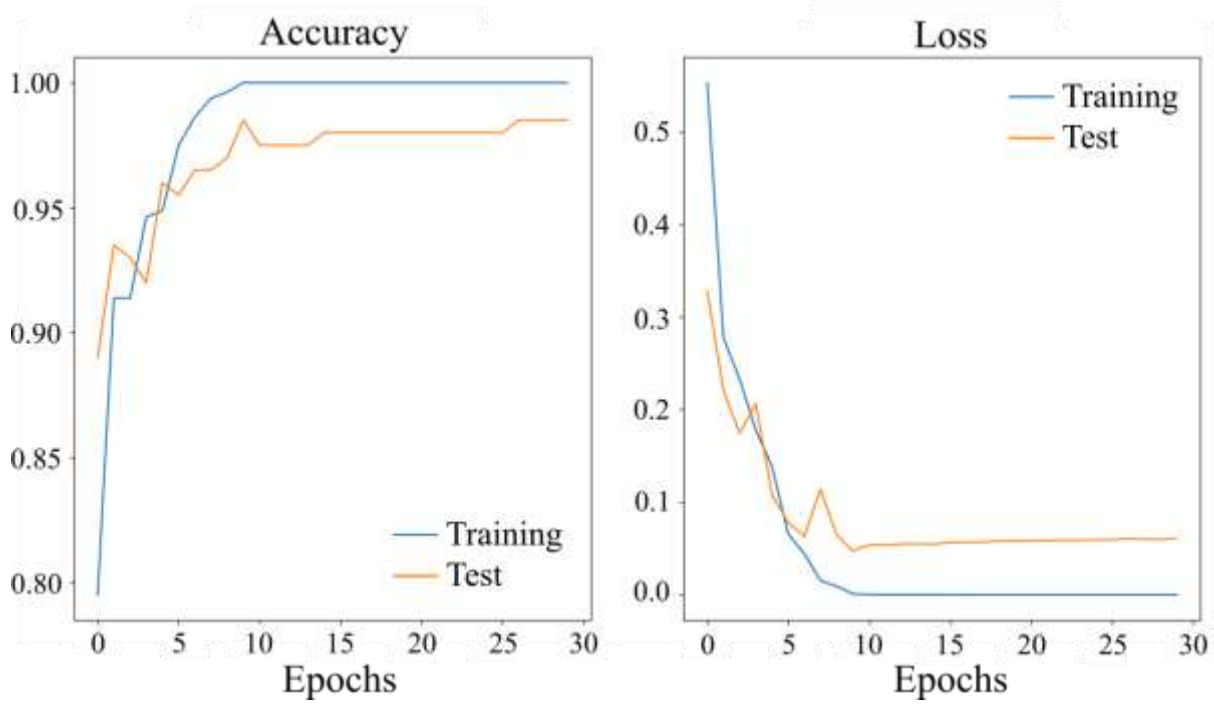

Fig. 14: Trend of loss and accuracy depending on the number of epochs.

3.3. Results using 240-image dataset

The CNN performance was evaluated for the different acquisition methods, using two datasets, each of 240 images, containing ground-based operator and UAV images. For both datasets, 144 different CNN configurations were obtained by varying the pre-processing types (Thresholding, Wavelet, Box Blur and Sobel Feldman); the optimizer selection (SGD, Adam); the model types (0, 1, 3), the size of the image 3 kpx; the batch (5, 10) and kernel size (3, 5), and number of filters ({16, 32, 32, 64, 128}, {32, 64, 128, 256}). As for the results of the previous tests, the number of epochs was kept at 60. Tests on images acquired by ground-based operators allowed an accuracy of 93% to be obtained. UAV images, instead, allowed an accuracy of 98% to be obtained. The best configurations are shown in Tab. 7. Tests carried out with UAV images provided the best classification performance for "Operative" images with an accuracy of 100%, while the images in the "Hotspot" category had accuracy values of 97% and 94%.

Table 7: Extract of best configurations for different tests.

	Confusion Matrix

Please cite this paper as:
D. Manno, G. Cipriani, G. Ciulla, V. Di Dio, S. Guarino, V. Lo Brano. (2021). Deep learning strategies for automatic fault diagnosis in photovoltaic systems by thermographic images. Energy Conversion and Management, 241, 114315.
https://doi.org/10.1016/j.enconman.2021.114315

	pp	Opt	m	b	k	f	Duration (s)	TP	FP	FN	TN	Accuracy
UAV	TH	Adam	1	10	3	32	162	30	0	1	29	0.98
	TH	Adam	3	5	5	32	282	30	0	1	29	0.98
	TH	Adam	0	5	5	32	281	30	0	2	28	0.97
Operator	TH	Adam	0	5	5	16	172	27	3	1	29	0.93
	WA	Adam	3	5	5	32	303	29	1	3	27	0.93
	TH	SGD	0	5	5	16	161	26	4	1	29	0.92
								Operative		Hotspot		

Legend: *pp = pre-processing, e = number of epochs, opt = optimizer, m = model, b = batch size, img = image size, k = kernel size, f = filter size, TH = thresholding, WA = DWT.*

The tests carried out with the UAV image dataset resulted in a maximum accuracy of 93%, with an accuracy of 97% for the "Operative" class while the images acquired by an operator were characterized by a maximum value of 85%. In the ROC space represented in Fig. 15, the CNN performances for each class were compared with datasets acquired by a ground-based operator and UAV. The "Operative" images of the UAV dataset were classified for 12% of the total tests with a zero error, while the CNN high-sensitivity operative point was not reached for the images acquired by a ground-based operator. Comparing tests with UAV and operator images, 16.7% and 9% of the total tests achieved random or worse performance results, respectively.

Please cite this paper as:
D. Manno, G. Cipriani, G. Ciulla, V. Di Dio, S. Guarino, V. Lo Brano. (2021). Deep learning strategies for automatic fault diagnosis in photovoltaic systems by thermographic images. Energy Conversion and Management, 241, 114315.
https://doi.org/10.1016/j.enconman.2021.114315

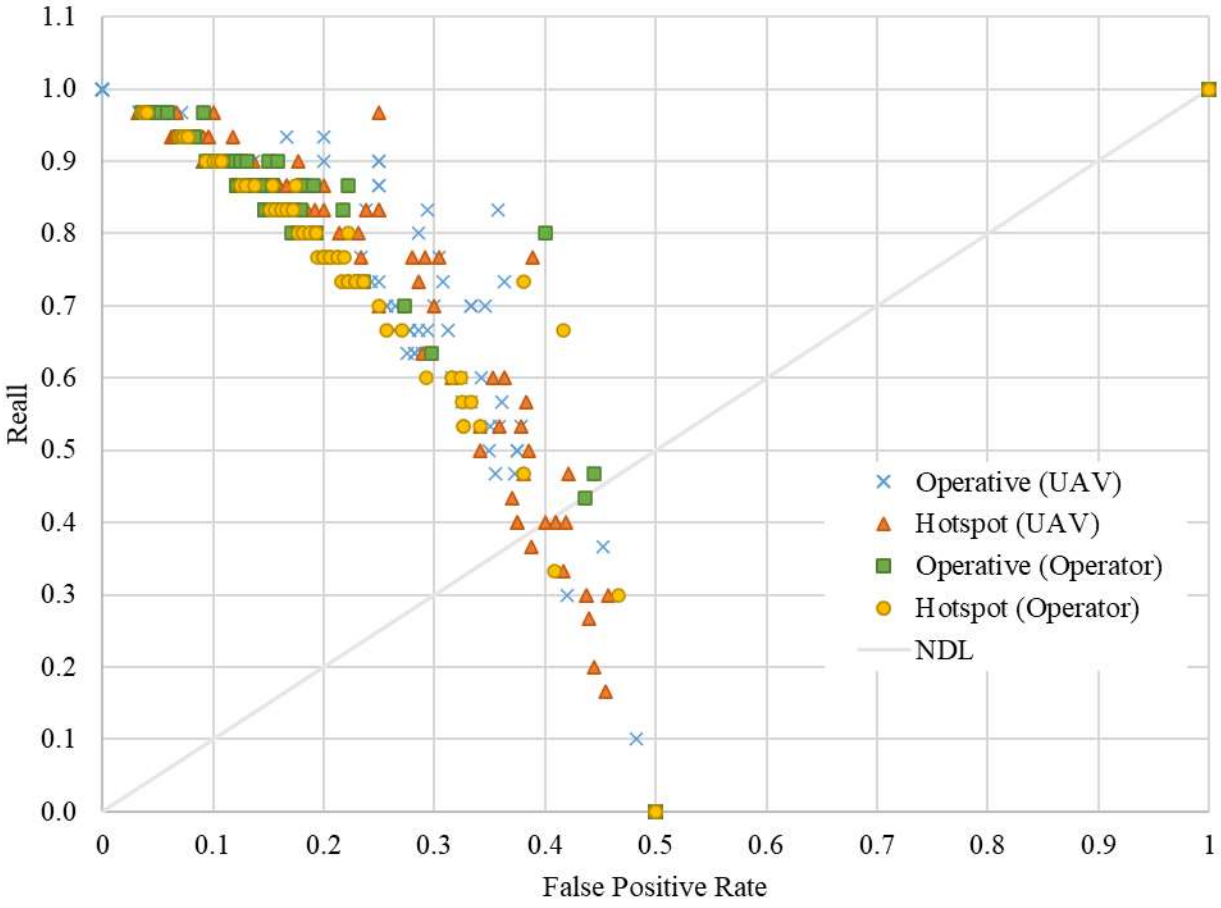

Fig. 15: ROC space for 240-image dataset.

The same configurations were replicated using different augmentation techniques, which made it possible to multiply the training images by a factor of five. The CNN performances were decreased with the application of augmentation techniques, as shown in the ROC space in Fig. 16. In fact, the random or worse performance results increased by 11.3% and 11%, respectively, using UAV and operator images.

Please cite this paper as:
D. Manno, G. Cipriani, G. Ciulla, V. Di Dio, S. Guarino, V. Lo Brano. (2021). Deep learning strategies for automatic fault diagnosis in photovoltaic systems by thermographic images. Energy Conversion and Management, 241, 114315.
https://doi.org/10.1016/j.enconman.2021.114315

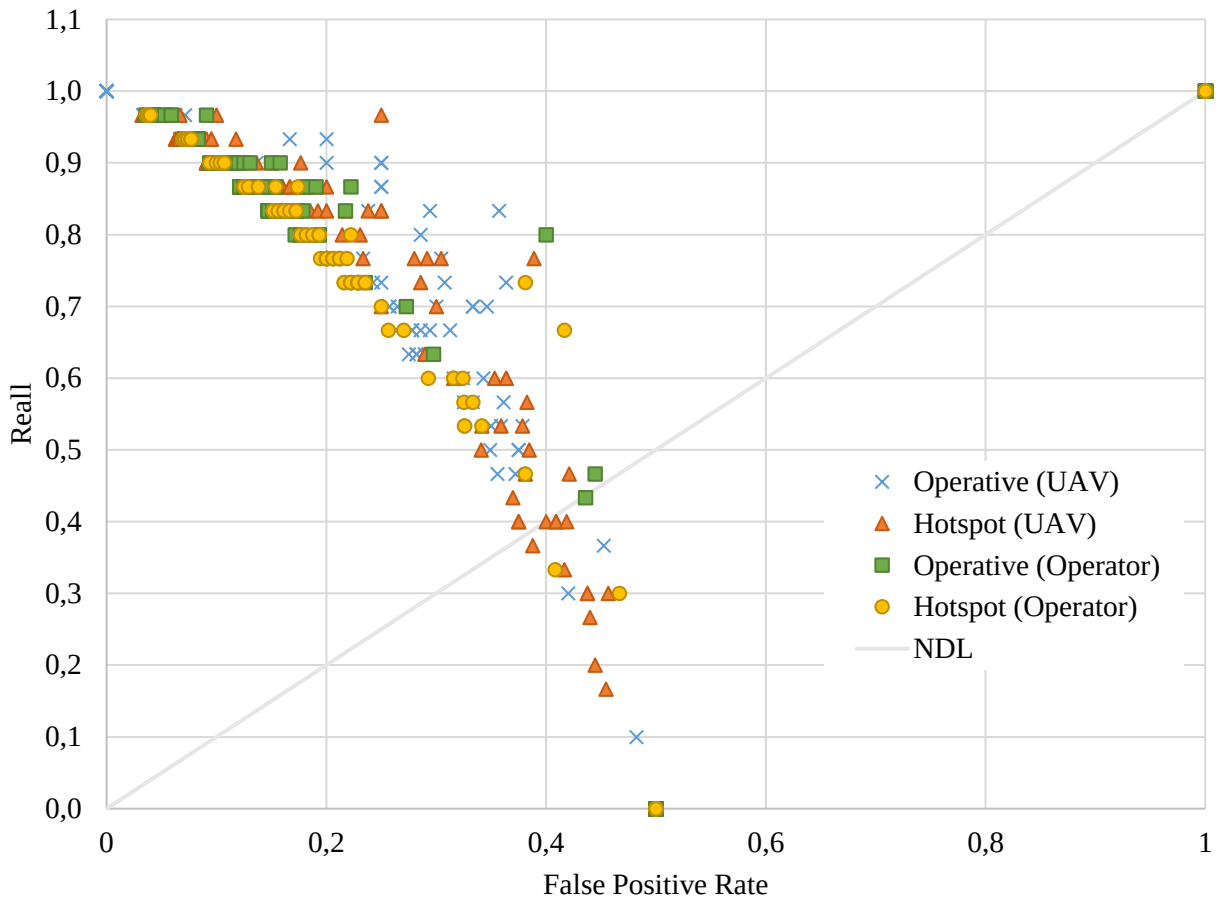

Fig. 16: ROC space for 240-image dataset with augmentation techniques.

3.4. Results using 200 sectioned image dataset

To evaluate the performance of the CNN with an MLP architecture, 12 identical tests were performed using: RGB and Thresholding pre-processing types; stochastic optimizers (respectively SGD and Montecarlo); a hyperbolic tangent activation function; batch size of 5 and number of epochs of 15, 30 and 60. For all configurations, images containing 375 pixels were used. To execute this test, a CNN with 3 Convolutional layers, kernel size of 3, and number of filters {16, 32, 64} were used. The benchmarking of the results is shown in Tab. 8. The classification of sectioned images achieved the best performance of CNN with 100% accuracy, thanks to the simplification of the complexity of the images. From the test results for the classification problem, the performance of CNN is much higher than that of MLPs, which achieved 90% accuracy for the same test.

Please cite this paper as:
D. Manno, G. Cipriani, G. Ciulla, V. Di Dio, S. Guarino, V. Lo Brano. (2021). Deep learning strategies for automatic fault diagnosis in photovoltaic systems by thermographic images. Energy Conversion and Management, 241, 114315.
https://doi.org/10.1016/j.enconman.2021.114315

Table 8: Comparison between MLP and CNN extract of results.

		Convolutional Neural Network			Multi-Layer Perceptron		
Pre-processing	Epochs	Duration (s)	Accuracy	FS_{AVG}	Duration (s)	Accuracy	FS_{AVG}
Thresholding	15	14.604	1	1	25.963	0.9	0.9
Thresholding	30	27.582	1	1	43.356	0.9	0.9
Thresholding	60	55.607	1	1	49.137	0.9	0.9

CNN provided results very close to the ideal behavior of the classifier, obtaining the best classification performance for each of the classes, as shown in Fig. 17. This last figure displays the accuracy and loss trends in the test and training phases: the total overlap of the curves indicates the ideal CNN behavior without overfitting. The trend of the accuracy in the training phase reaches 1 in 2 epochs, while in the test phase from the 1st epoch it remains constant at 1. The loss trend, instead, decreases to zero with an exponential trend both in the training and testing phase.

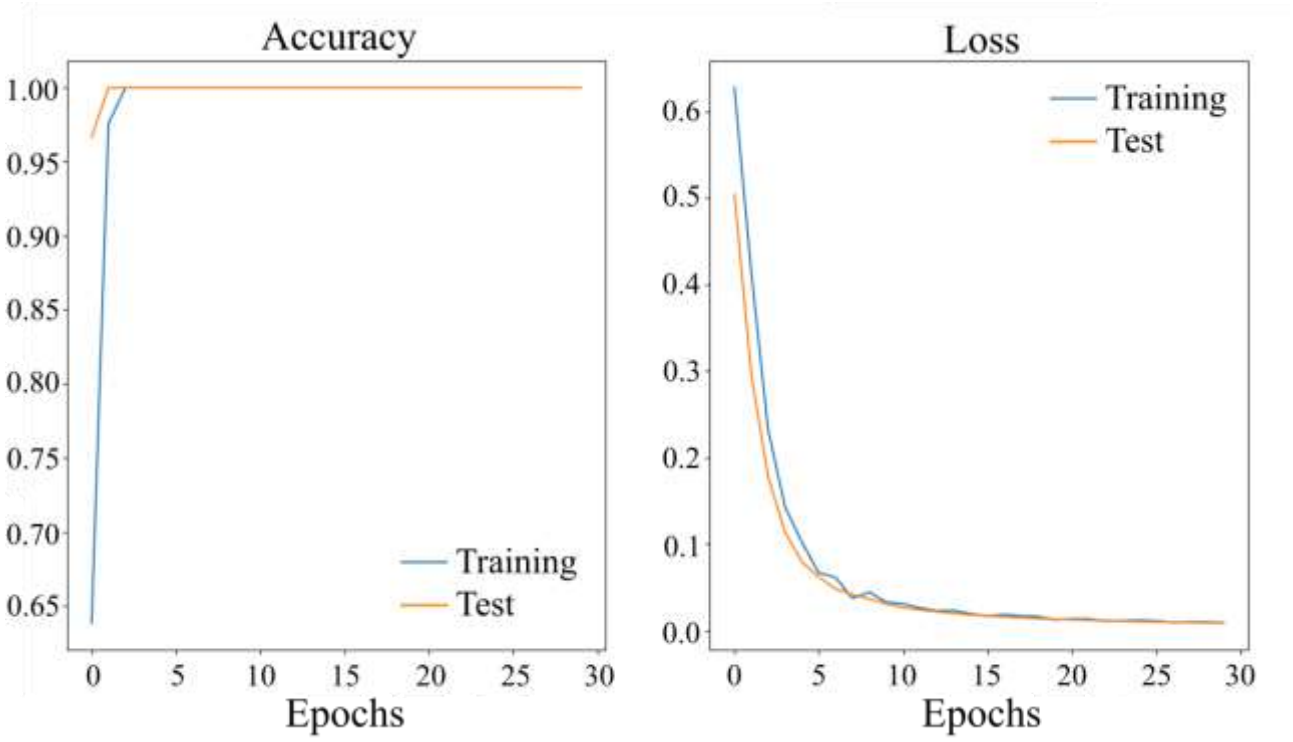

Please cite this paper as:
D. Manno, G. Cipriani, G. Ciulla, V. Di Dio, S. Guarino, V. Lo Brano. (2021). Deep learning strategies for automatic fault diagnosis in photovoltaic systems by thermographic images. Energy Conversion and Management, 241, 114315.
https://doi.org/10.1016/j.enconman.2021.114315

Fig. 17: Accuracy and loss trends for the CNN test.

4. Discussions

The identification of thermographic images acquired for PV modules can be carried out automatically using the proposed CNN made on open-source systems, with the architectures and parameters indicated in this paper. As shown by the results related to the 1000-image dataset and the 200 sectioned image dataset, CNN allowed image classification in a simple and fast way and with a high degree of accuracy. The dataset consists of thermographic images with different characteristics that allowed CNN, through supervised training, to identify the necessary characteristics for the classification of the images into two classes. These characteristics are highlighted by the use of pre-processing techniques, which, as demonstrated by the various tests carried out, reduce the presence of noise and limit the time required to perform the tests. The same tests performed with the 500-image dataset and with the same characteristics show a similar computational time for pre-processed grayscaling, thresholding, and DWT, but a 26% increase of execution time for the application of Box blur and Sobel Feldman filters and 67.59% for color images.

Comparing the tests executed with the various configurations, the use of color images does not allow high CNN performances, reaching an FS_{AVG} value of 61.8% for the dataset of 500 images. Similar results from DWT, Grayscale, and Box blur - Sobel Feldman filters are obtained with FS_{AVG} from 62% to 67%. Instead, Thresholding removes most of the unnecessary features for identifying images in the two classes. For the image sets used, artifacts (noise) that can be misclassified as “Hotspots” by CNN are overheated junction boxes and drone reflection on the modules. Conversely, images with small hotspots, attributable to a few pixels, can be misclassified as “Operative”. The presence of noise that causes classification error is overcome in the sectioning of the thermographic images, obtaining an FS_{AVG} of 100%, despite using a small dataset. According to the results obtained with the 240-image dataset, consisting of UAV and ground-based operator images, the use of datasets with a lower image variety reduced the CNN performance by 2% and 6% respectively, compared to the 1000-image dataset. The augmentation techniques applied to the images increased the number of classification errors in both classes, due to the different quality of the input images such as different resolution, framing, presence of foreign objects in the image, and noise. According to the results obtained using the 240-image dataset, UAV-acquired images provided better CNN performance than

Please cite this paper as:
D. Manno, G. Cipriani, G. Ciulla, V. Di Dio, S. Guarino, V. Lo Brano. (2021). Deep learning strategies for automatic fault diagnosis in photovoltaic systems by thermographic images. Energy Conversion and Management, 241, 114315.
https://doi.org/10.1016/j.enconman.2021.114315

images captured manually by a ground-based operator, which can be subject to human error. Also, for UAV images pre-processed using augmentation techniques, there was a 12% higher misclassification in the "Hotspot" category, due to the causal application of roto-translation and zooming techniques, which may exclude parts of the image containing essential features for the recognition of hotspot. The CNN performance was also affected by the different models used. Model "2" caused a decrease in FS_{AVG} between 6% and 9%, due to the dropout layer which stochastically eliminated input information to reduce the overfitting problem, making the CNN prone to more errors. The use of this layer was not advantageous for the tests performed, as the variety of images used to compose the datasets limited the CNN fitting. Models "0" and "1" using the ReLU activation function allowed for higher performances at each image resizing, while the use of models "3" and "4" with Sigmoid and Hyperbolic tangent activation function allowed for lower performances due to the distribution of the features.

The comparison between the results obtained by the proposed CNN models and a more classical MLP corroborated the better performance of CNN for thermographic image classification. In the literature, several applications of CNN for image classification are available. Four works [34,77–79] concerning the classification of thermographic images on photovoltaic modules, carried out in 2020, are compared in Tab. 9.

Please cite this paper as:
D. Manno, G. Cipriani, G. Ciulla, V. Di Dio, S. Guarino, V. Lo Brano. (2021). Deep learning strategies for automatic fault diagnosis in photovoltaic systems by thermographic images. Energy Conversion and Management, 241, 114315.
https://doi.org/10.1016/j.enconman.2021.114315

Table 9: Comparison of different works using CNN for classification of thermographic images.

Reference of study	**Present work**	**Herraiz et al.** [77]	**Pierdicca et al.** [34]	**Du et al.** [78]	**Espinosa et al.** [79]
Image acquisition equipment	ground-based operator and UAV	Drone DJI S900	FLIR TAU 2	FLIR A310 in permanent position	-
Image resolution	various	640x354	640x512	320x240	200x200
Number of images	· 1000 and 500 images datasets · 2 datasets of 240 images, each of them collected by operator and UAV only · 200 sectioned image datasets	· 800 for training · 100 for testing and validation	· 1622 for balance dataset · 3336 for unbalance dataset	1440	· 140 for 2 classes · 200 for 4 classes
Classification classes	operative, hotspot	hotspot	fault, no-fault	brocken edge, surface impurity, scratch, crack, hotspot, large area damage	fault, no-fault and fault, no-fault, dust, shadows
Pre-processing procedure	· resize · homogenization and normalization · RGB · DWT · grayscale · thresholding · Sobel Feldman and box blur filters · augmentation techniques	· image rotation · Sobel Feldman filter	· grayscale · resize · augmentation techniques	· resize · features extractions algorithm	resize
Algorithm architecture	model “0”, “1”, “2”, “3”,”4” displayed in section 2.3	single-classification architecture: · 3 convolutional layers · filter size · Maxpooling and Average-pooling layer · ReLu activation function	VGG-16 standard architecture	VGG-16, Le Net-5 and GoogleLeNet standard architecture	binary classification architecture: · 4 convolutional layers · Maxpooling · ReLu activation function multy-classification architecture: · 5 convolutional layers · Maxpooling · ReLu activation function
Results	· 97% accuracy for 500 images datasets · 99% accuracy for 1000 images datasets · 98% accuracy for 240 images datasets acquired by UAV · 93% accuracy for 240 images datasets acquired by ground-based operator with and without augmentation techniques · 97% accuracy for 240 images datasets acquired by UAV with augmentation techniques	92.25% accuracy	· 74% precision for balance datasets · 70% for balance datasets with augmentation tecniques · 57% precision for unbalance datasets	· 97.68% accuracy with resize · 97.92% accuracy with features extractions	· 75.39% accuracy for faults · 70% accuracy for no-fault · 65.71% accuracy for dust · 41.03% accuracy for shadows

Please cite this paper as:
D. Manno, G. Cipriani, G. Ciulla, V. Di Dio, S. Guarino, V. Lo Brano. (2021). Deep learning strategies for automatic fault diagnosis in photovoltaic systems by thermographic images. Energy Conversion and Management, 241, 114315.
https://doi.org/10.1016/j.enconman.2021.114315

	· 100% accuracy for sectioned image dataset				
Deep leaning platform	Tensorflow and Keras	Tensorflow	Tensorflow and Keras	Caffè	Deep learning toolbox MATLAB

Please cite this paper as:
D. Manno, G. Cipriani, G. Ciulla, V. Di Dio, S. Guarino, V. Lo Brano. (2021). Deep learning strategies for automatic fault diagnosis in photovoltaic systems by thermographic images. Energy Conversion and Management, 241, 114315.
https://doi.org/10.1016/j.enconman.2021.114315

Table 9 compares the methodologies used in these works, the equipment for the acquisition of thermographic images, the characteristics of the datasets (number of images, resolution), the pre-processing techniques, the number of classes, the algorithm architecture, the results, and the framework used. The works used comparable logic algorithms developed with similar architecture in different deep learning platforms (TensorFlow, Keras, Caffè, and Matlab). The algorithms employ equal activation and pooling functions, and the numbers of fully connected layers are comparable. Hence, perceptrons are trained similarly using inputs processed by the same mathematical functions. Models "3" and "4" use different activation functions to evaluate the performance of CNN with different configurations from those commonly used. Unlike the compared architectures, model "2" contains the Dropout layer to limit data overfitting.

The comparison of these works shows that methodologies are less performing than those proposed in this paper although the structure of the CNN employed is basic. The learning capabilities of CNN are not maximized using thermographic images referring to a single site nor are they acquired using only one type of equipment as in the tests performed in this research. Besides, the types of pre-processing used in the other works highlight the recognition characteristics of the thermographic image in a limited way and do not completely eliminate noise.

5. Conclusions

The automatic classification of thermographic images is an efficient and fast method to diagnose the operating status of a PV module, avoiding the loss of electricity production due to the reduced efficiency of the system. The availability and cost-effectiveness of the proposed method will allow widespread use of the system by unqualified operators for the recognition of thermographic images, limiting human error. The algorithm proposed by the authors allows the automatic recognition of thermographic images acquired using different equipment (by a ground-based operator or through the use of Unmanned Areal Vehicles) without following a standard protocol that often makes this process time-consuming and complex. This result is achieved by using various pre-processing strategies for noise reduction and highlighting image features, including normalization and homogenization of pixels, greyscaling, Thresholding, Discrete Wavelet Transform, Sobel Feldman and Box blur filtering. In more detail, using the threshold as a pre-processing methodology enabled the best performance of the CNN, achieving 99% accuracy with less than 30 minutes computational time on

Please cite this paper as:
D. Manno, G. Cipriani, G. Ciulla, V. Di Dio, S. Guarino, V. Lo Brano. (2021). Deep learning strategies for automatic fault diagnosis in photovoltaic systems by thermographic images. Energy Conversion and Management, 241, 114315.
https://doi.org/10.1016/j.enconman.2021.114315

Low Mid -Range CPU. Furthermore, the simplification of the thermographic images, which refers to multiple operating states of the PV modules, has allowed the achievement of high accuracy; considering a dataset of 200 sectioned images, the same configuration obtained an accuracy of 90% for an MLP network and 100% for a CNN.

The best performances of CNN were obtained with the configuration consisting of pre-processing Threshold, 30 epochs, Adam optimizer, model "1", 5 or 10 batch size, 12096 image size, 3 kernel size and {32, 64, 128, 256} filter size. Augmentation techniques and the Dropout layer were introduced to reduce overfitting, but according to the results, these techniques do not provide substantial improvements, and can even cause a decrease in accuracy by a few percentage points.

Regarding the performance of Thermographic Non-Destructive Testing with Unmanned Areal Vehicle support, this choice allows the inspection of a greater number of PV modules than the same test performed on the ground by a qualified operator, thereby saving time. The performance of CNN was evaluated by comparing both acquisition types of thermographic images: the Unmanned Areal Vehicle thermographic images allow an accuracy greater than 5% of ground-based operator images, achieving 98% accuracy in 2.4 minutes using 240-image datasets. Therefore, the use of Thermographic Non-Destructive Tests supported by Unmanned Areal Vehicles and CNN proposed in this paper allows a considerable reduction in the investigation times of PV modules with consequent prompt resolution of the abnormal operating conditions accelerating the diagnosis phase.

As is underlined in these results, the work proposes a methodology that overcomes the limits shown by other approaches present in the literature and guarantees a higher degree of reliability. Based on this, the proposed methodology stands as an alternative and valid tool that improves the resolution of image classification problems and can be used in any scientific field or sector.

This work represents the first phase of a more complete and more detailed vision. In future work, the acquisition of thermographic images of a single PV module will be investigated by Thermographic Non-Destructive Test supported by Unmanned Areal Vehicle and CNN, for real-time fault classification according to their severity. The idea is to create a user-friendly application available to PV plant managers that identifies, by overflying the PV modules, the presence of faults and promptly intervene to reduce energy loss. Additionally, the proposed approach can be used in areas where visual inspection for status detection is effective, such as identifying abnormal operation of an

Please cite this paper as:
D. Manno, G. Cipriani, G. Ciulla, V. Di Dio, S. Guarino, V. Lo Brano. (2021). Deep learning strategies for automatic fault diagnosis in photovoltaic systems by thermographic images. Energy Conversion and Management, 241, 114315.
https://doi.org/10.1016/j.enconman.2021.114315

electrical machine by detecting heat distribution with infrared thermography and classifying the severity of joule losses detected during the inspection.

Acknowledged

The companies that provided the thermographic images are thanked: Atlante snc., REA s.r.l, SAIGE S.a.S, Andrea Carlini, Stefano Carponi.

Nomenclature

A	accuracy (%)
b	bias vector
CO_2	Carbon dioxide
$f(n)$	input matrix (image)
FS	f-score [%]
FN	number of false negative samples
FP	number of false positive samples
FPR	number of false positive rate
$g(n)$	convolution matrix (Kernel)
K	Kernel size
N	Kernel strides
P	padding value
R	recall (%)
s	activaction function
SO_2	Sulfur dioxide
TN	number of true negative samples
TP	number of true positive samples

Please cite this paper as:
D. Manno, G. Cipriani, G. Ciulla, V. Di Dio, S. Guarino, V. Lo Brano. (2021). Deep learning strategies for automatic fault diagnosis in photovoltaic systems by thermographic images. Energy Conversion and Management, 241, 114315.
https://doi.org/10.1016/j.enconman.2021.114315

W'	size of the activation map function
W	two-dimensional matrix containing the number of neurons of the previous and current layer
x	input vector

Abbreviations

AI	Artificial Intelligence
CNN	Convolutional Neural Network
DCNN	Deep Convolutional Neural Network
DWT	Discrete Wavelet Transform
MLP	Multy-Layer Perceptrons
NDL	Non-Discrimination Line
PV	Photovoltaic
ROC	Receiver Operating Characteristic
SGD	Stochastic Gradient Descent
SVM	Support Vector Machines
TNDT	Thermographic Non-Destructive Test
UAV	Unmanned Areal Vehicle

References

[1] IRENA. Renewable Energy Statistics 2020. 2020.

[2] Abas N, Kalair A, Khan N. Review of fossil fuels and future energy technologies. Futures 2015;69:31–49.

[3] Alsema E. Energy payback time and CO2 emissions of PV systems. Pract. Handb. Photovoltaics, Elsevier; 2012, p. 1097–117.

Please cite this paper as:
D. Manno, G. Cipriani, G. Ciulla, V. Di Dio, S. Guarino, V. Lo Brano. (2021). Deep learning strategies for automatic fault diagnosis in photovoltaic systems by thermographic images. Energy Conversion and Management, 241, 114315.
https://doi.org/10.1016/j.enconman.2021.114315

[4] Reinsberger K, Posch A. Bottom-up initiatives for photovoltaic: incentives and barriers. J Sustain Dev Energy, Water Environ Syst 2014;2:108–17.

[5] Hernández-Moro J, Mart\'\inez-Duart JM. Economic analysis of the contribution of photovoltaics to the decarbonization of the power sector. Renew Sustain Energy Rev 2015;41:1288–97.

[6] GA UN. Transforming our world: the 2030 Agenda for Sustainable Development. Div Sustain Dev Goals New York, NY, USA 2015.

[7] Sobri S, Koohi-Kamali S, Rahim NA. Solar photovoltaic generation forecasting methods: A review. Energy Convers Manag 2018;156:459–97.

[8] Murdock HE, Gibb D, André T, Appavou F, Brown A, Epp B, et al. Renewables 2019 global status report 2019.

[9] GSE. Solare fotovoltaico -Rapporto statistico. GSE 2018.

[10] Jäger-Waldau A. Snapshot of Photovoltaics—February 2020. Energies 2020;13:930.

[11] Jordan DC, Silverman TJ, Wohlgemuth JH, Kurtz SR, VanSant KT. Photovoltaic failure and degradation modes. Prog Photovoltaics Res Appl 2017. doi:10.1002/pip.2866.

[12] Capparella S, Falvo MC. Secure faults detection for preventing fire risk in PV systems. 2014 Int. Carnahan Conf. Secur. Technol., 2014, p. 1–5.

[13] Köntges M, Kurtz S, Packard CE, Jahn U, Berger K, Kato K, et al. Review of Failures of Photovoltaic Modules. 2014. doi:978-3-906042-16-9.

[14] Dubey S, Sarvaiya JN, Seshadri B. Temperature dependent photovoltaic (PV) efficiency and its effect on PV production in the world--a review. Energy Procedia 2013;33:311–21.

[15] Skomedal ÅF, Aarseth BL, Haug H, Selj J, Marstein ES. How much power is lost in a hot-spot? A case study quantifying the effect of thermal anomalies in two utility scale PV power plants. Sol Energy 2020;211:1255–62.

[16] Mellit A, Tina GM, Kalogirou SA. Fault detection and diagnosis methods for photovoltaic systems: A review. Renew Sustain Energy Rev 2018;91:1–17.

[17] Herrmann W, Wiesner W, Vaassen W. Hot spot investigations on PV modules-new concepts

Please cite this paper as:
D. Manno, G. Cipriani, G. Ciulla, V. Di Dio, S. Guarino, V. Lo Brano. (2021). Deep learning strategies for automatic fault diagnosis in photovoltaic systems by thermographic images. Energy Conversion and Management, 241, 114315.
https://doi.org/10.1016/j.enconman.2021.114315

for a test standard and consequences for module design with respect to bypass diodes. Conf. Rec. Twenty Sixth IEEE Photovolt. Spec. Conf., 1997, p. 1129–32.

[18] King DL, Kratochvil JA, Quintana MA, McMahon TJ. Applications for infrared imaging equipment in photovoltaic cell, module, and system testing. Conf. Rec. Twenty-Eighth IEEE Photovolt. Spec. Conf. (Cat. No. 00CH37036), 2000, p. 1487–90.

[19] Hocine L, Samira KM, Tarek M, Salah N, Samia K. Automatic detection of faults in a photovoltaic power plant based on the observation of degradation indicators. Renew Energy 2021;164:603–17.

[20] Pei T, Li L, Zhang J, Hao X. Module block fault locating strategy for large-scale photovoltaic arrays. Energy Convers Manag 2020;214:112898.

[21] Tsanakas JA, Ha L, Buerhop C. Faults and infrared thermographic diagnosis in operating c-Si photovoltaic modules: A review of research and future challenges. Renew Sustain Energy Rev 2016;62:695–709.

[22] Usamentiaga R, Venegas P, Guerediaga J, Vega L, Molleda J, Bulnes FG. Infrared thermography for temperature measurement and non-destructive testing. Sensors 2014;14:12305–48.

[23] Acciani G, Falcone O, Vergura S. Typical Defects of PV-cells. 2010 IEEE Int. Symp. Ind. Electron., 2010, p. 2745–9.

[24] Madeti SR, Singh SN. A comprehensive study on different types of faults and detection techniques for solar photovoltaic system. Sol Energy 2017;158:161–85.

[25] Chen Z, Chen Y, Wu L, Cheng S, Lin P, You L. Accurate modeling of photovoltaic modules using a 1-D deep residual network based on IV characteristics. Energy Convers Manag 2019;186:168–87.

[26] Tanaka T, Hayashi T, Nagayama T, Yanagidaira T, Inui Y. Proposal of novel degradation diagnosis method for photovoltaic module employing xenon flash lighting system and detector capacitor. Energy Convers Manag 2019;186:450–61.

[27] Quater PB, Grimaccia F, Leva S, Mussetta M, Aghaei M. Light Unmanned Aerial Vehicles (UAVs) for cooperative inspection of PV plants. IEEE J Photovoltaics 2014;4:1107–13.

Please cite this paper as:
D. Manno, G. Cipriani, G. Ciulla, V. Di Dio, S. Guarino, V. Lo Brano. (2021). Deep learning strategies for automatic fault diagnosis in photovoltaic systems by thermographic images. Energy Conversion and Management, 241, 114315.
https://doi.org/10.1016/j.enconman.2021.114315

[28] Muntwyler U, Schuepbach E, Lanz M. Infrared (IR) drone for quick and cheap PV inspection. Proc. 31st Eur. Photovolt. Sol. Energy Conf. Exhib., 2015, p. 1804–6.

[29] Jahn U, Herz M, Köntges M, Parlevliet D, Paggi M, Tsanakas I. Review on infrared and electroluminescence imaging for PV field applications: International Energy Agency Photovoltaic Power Systems Programme: IEA PVPS Task 13, Subtask 3.3: report IEA-PVPS T13-12: 2018. International Energy Agency; 2018.

[30] de Oliveira AKV, Aghaei M, Rüther R. Aerial infrared thermography for low-cost and fast fault detection in utility-scale PV power plants. Sol Energy 2020;211:712–24.

[31] Commission IE, others. IEC TS 62446-3-Photovoltaic (PV) systems-Requirements for testing, documentation and maintenance-Part 3: Photovoltaic modules and plants-Outdoor infrared thermography. IEC, Geneva, Switz 2017.

[32] Kurukuru VSB, Haque A, Khan MA, Tripathy AK. Fault classification for photovoltaic modules using thermography and machine learning techniques. 2019 Int. Conf. Comput. Inf. Sci., 2019, p. 1–6.

[33] Gomathy B, Venkatesan T, Muniraj C, Umashankar S, Sanjeevikumar P, Mihet-Popa L. Infrared Thermography Based Defects Testing of Solar Photovoltaic Panel with Fuzzy Rule-Based Evaluation. Energies 2020;13:1343.

[34] Pierdicca R, Malinverni ES, Piccinini F, Paolanti M, Felicetti A, Zingaretti P. DEEP CONVOLUTIONAL NEURAL NETWORK FOR AUTOMATIC DETECTION OF DAMAGED PHOTOVOLTAIC CELLS. Int Arch Photogramm Remote Sens Spat Inf Sci 2018;42.

[35] Ciulla G, D'Amico A, Lo Brano V, Traverso M. Application of optimized artificial intelligence algorithm to evaluate the heating energy demand of non-residential buildings at European level. Energy 2019;176. doi:10.1016/j.energy.2019.03.168.

[36] Culberson JC. On the futility of blind search: An algorithmic view of "no free lunch." Evol Comput 1998;6:109–27.

[37] Partridge D. Artificial intelligence. Curated Ref. Collect. Neurosci. Biobehav. Psychol., 2016. doi:10.1016/B978-0-12-809324-5.02995-3.

Please cite this paper as:
D. Manno, G. Cipriani, G. Ciulla, V. Di Dio, S. Guarino, V. Lo Brano. (2021). Deep learning strategies for automatic fault diagnosis in photovoltaic systems by thermographic images. Energy Conversion and Management, 241, 114315.
https://doi.org/10.1016/j.enconman.2021.114315

[38] Metaxiotis K, Kagiannas A, Askounis D, Psarras J. Artificial intelligence in short term electric load forecasting: a state-of-the-art survey for the researcher. Energy Convers Manag 2003;44:1525–34.

[39] Lo Brano V, Ciulla G, Di Falco M. Artificial neural networks to predict the power output of a PV panel. Int J Photoenergy 2014;2014.

[40] Garoudja E, Chouder A, Kara K, Silvestre S. An enhanced machine learning based approach for failures detection and diagnosis of PV systems. Energy Convers Manag 2017;151:496–513.

[41] Ciulla G, D'Amico A, Di Dio V, Lo Brano V. Modelling and analysis of real-world wind turbine power curves: Assessing deviations from nominal curve by neural networks. Renew Energy 2019;140. doi:10.1016/j.renene.2019.03.075.

[42] Kotsiantis SB, Zaharakis I, Pintelas P. Supervised machine learning: A review of classification techniques. Emerg Artif Intell Appl Comput Eng 2007;160:3–24.

[43] Nilsson NJ. Principles of Artificial Intelligence. IEEE Trans Pattern Anal Mach Intell 1981. doi:10.1109/TPAMI.1981.4767059.

[44] O'Rourke J, Toussaint GT. Pattern recognition. Handb. Discret. Comput. Geom. Third Ed., 2017. doi:10.1201/9781315119601.

[45] Pattern Recognition and Machine Learning. J Electron Imaging 2007. doi:10.1117/1.2819119.

[46] Krizhevsky A, Sutskever I, Hinton GE. ImageNet classification with deep convolutional neural networks. Commun ACM 2017. doi:10.1145/3065386.

[47] Schmidhuber J. Deep Learning in neural networks: An overview. Neural Networks 2015. doi:10.1016/j.neunet.2014.09.003.

[48] LeCun Y, Bengio Y, others. Convolutional networks for images, speech, and time series. Handb Brain Theory Neural Networks 1995;3361:1995.

[49] Fukushima K, Miyake S. Neocognitron: A self-organizing neural network model for a mechanism of visual pattern recognition. Compet. Coop. neural nets, Springer; 1982, p. 267–

Please cite this paper as:
D. Manno, G. Cipriani, G. Ciulla, V. Di Dio, S. Guarino, V. Lo Brano. (2021). Deep learning strategies for automatic fault diagnosis in photovoltaic systems by thermographic images. Energy Conversion and Management, 241, 114315.
https://doi.org/10.1016/j.enconman.2021.114315

85.

[50] LeCun Y, Bengio Y, Hinton G. Deep learning. Nature 2015;521:436–44.

[51] Hubel DH, Wiesel TN. Receptive fields of single neurones in the cat's striate cortex. J Physiol 1959. doi:10.1113/jphysiol.1959.sp006308.

[52] Zeiler MD, Fergus R. Visualizing and understanding convolutional networks. Lect. Notes Comput. Sci. (including Subser. Lect. Notes Artif. Intell. Lect. Notes Bioinformatics), 2014. doi:10.1007/978-3-319-10590-1_53.

[53] Aghdam HH, Heravi EJ. Guide to Convolutional Neural Networks. New York, NY Springer Doi 2017;10:973–8.

[54] Zhang Q, Wu YN, Zhu SC. Interpretable Convolutional Neural Networks. Proc. IEEE Comput. Soc. Conf. Comput. Vis. Pattern Recognit., 2018. doi:10.1109/CVPR.2018.00920.

[55] Li J, Mei X, Prokhorov D, Tao D. Deep neural network for structural prediction and lane detection in traffic scene. IEEE Trans Neural Networks Learn Syst 2016;28:690–703.

[56] Kuo C-CJ. Understanding convolutional neural networks with a mathematical model. J Vis Commun Image Represent 2016;41:406–13.

[57] Jiang X, Pang Y, Li X, Pan J, Xie Y. Deep neural networks with Elastic Rectified Linear Units for object recognition. Neurocomputing 2018. doi:10.1016/j.neucom.2017.09.056.

[58] Dunne R, Campbell N. On the pairing of the Softmax activation and cross-entropy penalty functions and the derivation of the Softmax activation function. Proc 8th Aust Conf Neural Networks 1997. doi:10.1.1.49.6403.

[59] Zhang Q, Zhang M, Chen T, Sun Z, Ma Y, Yu B. Recent advances in convolutional neural network acceleration. Neurocomputing 2019. doi:10.1016/j.neucom.2018.09.038.

[60] Tetko I V, Livingstone DJ, Luik AI. Neural Network Studies. 1. Comparison of Overfitting and Overtraining. J Chem Inf Comput Sci 1995. doi:10.1021/ci00027a006.

[61] Nitish S, Geoffrey H, Alex K, Ilya S, Ruslan S. Dropout: A Simple Way to Prevent Neural Networks from Overfitting. J Mach Learn Res 2014. doi:10.1109/ICAEES.2016.7888100.

[62] Martín Abadi, Ashish Agarwal, Paul Barham, Eugene Brevdo, Zhifeng Chen, Craig Citro,

Please cite this paper as:
D. Manno, G. Cipriani, G. Ciulla, V. Di Dio, S. Guarino, V. Lo Brano. (2021). Deep learning strategies for automatic fault diagnosis in photovoltaic systems by thermographic images. Energy Conversion and Management, 241, 114315.
https://doi.org/10.1016/j.enconman.2021.114315

Greg S. Corrado, Andy Davis, Jeffrey Dean, Matthieu Devin, Sanjay Ghemawat, Ian Goodfellow, Andrew Harp, Geoffrey Irving, Michael Isard, Rafal Jozefowicz, Yangqing Jia, Lukasz Kaiser, Manjunath Kudlur, Josh Levenberg, Dan Mané, Mike Schuster, Rajat Monga, Sherry Moore, Derek Murray, Chris Olah, Jonathon Shlens, et al. TensorFlow: Large-Scale Machine Learning on Heterogeneous Systems 2015.

[63] Chollet F, Allaire JJ. Deep Learning mit R und Keras: Das Praxis-Handbuch von den Entwicklern von Keras und RStudio. MITP-Verlags GmbH & Co. KG; 2018.

[64] D'Amico A, Ciulla G, Traverso M, Lo Brano V, Palumbo E. Artificial Neural Networks to assess energy and environmental performance of buildings: An Italian case study. J Clean Prod 2019;239. doi:10.1016/j.jclepro.2019.117993.

[65] Ertam F. Data classification with deep learning using tensorflow. 2nd Int. Conf. Comput. Sci. Eng. UBMK 2017, 2017. doi:10.1109/UBMK.2017.8093521.

[66] Gonzalez RC, Woods RE, Masters BR. Digital Image Processing, Third Edition. J Biomed Opt 2009. doi:10.1117/1.3115362.

[67] Saravanan C. Color image to grayscale image conversion. 2010 Second Int. Conf. Comput. Eng. Appl., vol. 2, 2010, p. 196–9.

[68] Choi JY, Ro YM, Plataniotis KN. A comparative study of preprocessing mismatch effects in color image based face recognition. Pattern Recognit 2011. doi:10.1016/j.patcog.2010.08.020.

[69] Smith SM, Nichols TE. Threshold-free cluster enhancement: Addressing problems of smoothing, threshold dependence and localisation in cluster inference. Neuroimage 2009. doi:10.1016/j.neuroimage.2008.03.061.

[70] Jamil N, Sembok TMT, Bakar ZA. Noise removal and enhancement of binary images using morphological operations. Proc. - Int. Symp. Inf. Technol. 2008, ITSim, 2008. doi:10.1109/ITSIM.2008.4631954.

[71] Sobel I, Feldman G. A 3x3 isotropic gradient operator for image processing. Hart, P E Duda R O Pattern Classif Scene Anal 1973.

[72] Hummel RA, Kimia B, Zucker SW. Deblurring Gaussian blur. Comput Vision, Graph Image

Please cite this paper as:
D. Manno, G. Cipriani, G. Ciulla, V. Di Dio, S. Guarino, V. Lo Brano. (2021). Deep learning strategies for automatic fault diagnosis in photovoltaic systems by thermographic images. Energy Conversion and Management, 241, 114315.
https://doi.org/10.1016/j.enconman.2021.114315

Process 1987. doi:10.1016/S0734-189X(87)80153-6.

[73] Takahashi R, Matsubara T, Uehara K. Data Augmentation using Random Image Cropping and Patching for Deep CNNs. IEEE Trans Circuits Syst Video Technol 2019. doi:10.1109/tcsvt.2019.2935128.

[74] Shorten C, Khoshgoftaar TM. A survey on Image Data Augmentation for Deep Learning. J Big Data 2019. doi:10.1186/s40537-019-0197-0.

[75] Sokolova M, Lapalme G. A systematic analysis of performance measures for classification tasks. Inf Process Manag 2009. doi:10.1016/j.ipm.2009.03.002.

[76] Flach PA. The geometry of ROC space: understanding machine learning metrics through ROC isometrics. Proc. 20th Int. Conf. Mach. Learn., 2003, p. 194–201.

[77] Herraiz ÁH, Marugán AP, Márquez FPG. Photovoltaic plant condition monitoring using thermal images analysis by convolutional neural network-based structure. Renew Energy 2020;153:334–48.

[78] Du B, He Y, He Y, Duan J, Zhang Y. Intelligent classification of silicon photovoltaic cell defects based on eddy current thermography and convolution neural network. IEEE Trans Ind Informatics 2019;16:6242–51.

[79] Espinosa AR, Bressan M, Giraldo LF. Failure signature classification in solar photovoltaic plants using RGB images and convolutional neural networks. Renew Energy 2020;162:249–56.

Please cite this paper as:
D. Manno, G. Cipriani, G. Ciulla, V. Di Dio, S. Guarino, V. Lo Brano. (2021). Deep learning strategies for automatic fault diagnosis in photovoltaic systems by thermographic images. Energy Conversion and Management, 241, 114315.
https://doi.org/10.1016/j.enconman.2021.114315

View publication stats